DEPARTMENT OF MECHANICAL ENGINEERING

SOUTHERN UNIVERSITY
BATON ROUGE, LOUISIANA 70813

FINAL REPORT

ON NASA GRANT NGR 19-005-009

To

National Aeronautics and Space Administration

Submitted by: Robert L. Scott Jr.
Department of Mechanical Engineering
Southern University, Baton Rouge, Louisiana

May, 1974

Summary

An experimental apparatus was designed and used to measure the bidirectional reflectance of zinc oxide (New Jersey Zinc Company SP 500) in the spectrum 0.25 to 2.5 microns. Besides obtaining original data for ZnO that is similar in nature to other reported bidirectional reflectance, measurements were also made in the absorption region at 0.350 micron for which very little data is published for any material. The results indicate the nonspecular reflectance is essentially Lambert for wavelengths above 0.40 microns with the most deviation occuring for large source zenith angles. Below 0.400 microns the nonspecular reflectance is greater than Lambert in all directions and is greatest in the forward and backscatter directions. The ratio of the specular component to the nonspecular component at a zenith of 0 degrees was found to increase with source zenith and wavelength for wavelengths above 0.400 microns. Below 0.400 microns this ratio increases as wavelength decrease. (The specular component at 70 degrees is more than 50 times larger than the specular component at 30 degrees for all wavelengths). The variation of bidirectional reflectance with wavelength was found to have the characteristics absorption for ZnO for wavelength below 0.400 microns.

TABLE OF CONTENTS

LIST OF TABLES

LIST OF TABLES (CONTINUED)

LIST OF TABLES (CONTINUED)

LIST OF ILLUSTRATIONS

LIST OF ILLUSTRATIONS (CONTINUED)

INTRODUCTION AND LITERATURE SURVEY

A detailed formulation of radiative heat transfer problems involves the use of bidirectional reflectance. Except for very simple systems this formulation is very intricate. For this reason and the fact that bidirectional data are scarce, such a formulation is not in common use. However, with the development of the digital computer there have been numerical methods developed for detailed radiative investigations using the bidirectional reflectance.

Since computations using bidirectional reflectance are coming into use for spacecraft radiative studies, it is necessary to have reflectance data on the materials involved. Materials that are frequently studied are coatings which are used in controlling the thermal environment of spacecrafts. This study is primarily concerned with the bidirectional reflectance of zinc oxide which is one constituent commonly used for coatings.

Definition of Bidirectional Reflectance

It is possible to define the bidirectional reflectance as a ratio of reflected heat flux in some direction to the incident heat flux in a particular direction or the definition could be a ratio of intensities. A definition could also employ a combination of these.

The definitions used are those given in the discussion by Torrance and Sparrow at the end of the reference by Birkebak and Eckert (20).[1]

$$\rho_1(\psi,\zeta;\theta,\phi) = di_r(\psi,\zeta;\theta,\phi)/e_i(\psi,\zeta)$$
$$= di_r(\psi,\zeta;\theta,\phi)/i_i(\psi,\zeta)\cos(\theta)d\omega_i \qquad (1)$$

$$\rho_{ah}(\psi,\zeta) = de_{r,h}(\psi,\zeta)/e_i(\psi\ \zeta)$$

$$= \int_{2\pi}\rho_1(\psi,\zeta;\theta,\phi)\cos(\theta)d\omega_r \qquad (2)$$

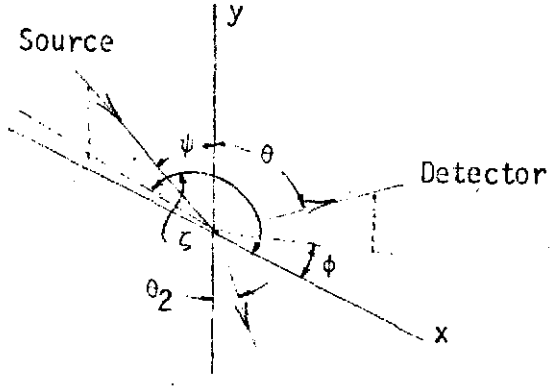

Figure 1. Coordinates

where

ρ_1 is the bidirectional reflectance,

ρ_{ah} is the angular hemispherical reflectance,

e_i is the incident energy,

d_{ir} is the reflected intensity,

i_i is the incident intensity,

$d\omega_i$ is the incident solid angle,

$d\omega_r$ is the reflected solid angle.

---

[1]The number in parenthesis corresponds to the reference in the bibliography.

The relative bidirectional reflectance is defined as

$$\rho_r(\psi,\zeta;\theta,\phi) = \frac{\rho_1(\psi,\zeta;\theta,\phi)}{\rho_1(\psi,\zeta;\theta_r,\phi_r)} \tag{3}$$

The reference direction (θ_r,ϕ_r) is chosen normal to the specimen surface. The detector signal which is a measure of reflected energy is denoted by $D(\psi,\zeta;\theta,\phi)$. In some instances for presentational simplicity the angles in parenthesis are omitted. The angles will always be given in degrees. Reflectance data is presented as relative values,

$$\rho_n(\psi,\zeta;\theta,\phi) = \frac{D(\psi,\zeta;\theta,\phi)}{D(\psi,\zeta;0°,\phi)} \tag{4}$$

and

$$\rho(\psi,\zeta;\theta,\phi) = \rho_n(\psi,\zeta;\theta,\phi)/\cos(\theta) \tag{5}$$

All reflectance measurements are made with monochromatic radiation and the micron (10^{-6} meters) is used for the unit of wavelength. Unless otherwise stated the term reflectance means bidirectional reflectance. A surface reflectance may obey Lambert's law in all directions except the specular direction where a distinguishable peak may exist. For this surface the diffuse reflectance is by definition Lambert's law. The specular reflectance is by definition the reflectance in the specular direction minus the diffuse reflectance in the specular direction. For a surface whose reflectance deviate from Lambert's law but has a distinguishable peak in the specular direction the diffuse reflectance is the reflectance minus the peak. The peak in the specular direction is the

specular reflectance. A perfect diffuser is a surface whose reflectance obeys Lambert's law and a plane reflector has zero diffuse reflectance. Units will conform to the International System of Units as given in NASA SP-7012.

Electromagnetic Theory of Reflectance

Ideally in a dissertation of this nature an analytical model of the problem is developed which describes the phenomena. However, due to the complex nature of the reflection from powder specimens theories have not been developed to explain the phenomena. Theories do exist for homogeneous conducting materials. It is felt that a better insight into the reflection phenomena of the subject specimen can be obtained from existing theories even though the theories are not directly applicable. This is true because the fundamental properties which are involved in reflection from homogeneous materials are also involved in reflection from powder specimens.

Several theories are used to explain light phenomena. If light interacts with matter whose dimensions are larger than its wavelength geometrical optics are used. If light interacts with matter whose dimensions are of the same order of magnitude as its wavelength, physical optics are used to explain the light phenomena and if light interacts with atomic entities of matter, quantum optics are used.

One of the important phenomena of physical optics which can affect the reflectance is diffraction. Basically this is the bending of light rays when there is an interaction of light with systens whose

dimensions are of the same order of magnitude as the light. This phenomenon is used to design diffraction gratings for high resolution monochromators. Electromagnetic theory can be used to predict the nature of light reflected from such a grating. This phenomenon is the principle reason geometrical optics may lead to erroneous results when used for reflectance predictions.

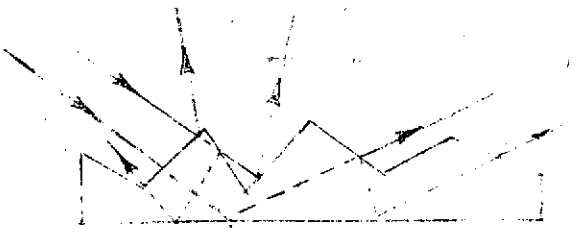

a. Homogeneous Material

b. Powder

Figure 2. Reflection from Rough Surfaces

Figure 2 shows reflection, shadowing and multiple scattering of a homogeneous material and a powder. Both materials are said to be rough because the surface asperities are involved in the reflection phenomena. For the powder it is necessary to distinguish between an asperity and a particle. A particle is the same as a crystal of ZnO and it's size is a measure of it's length for elongated particles

and a measure of it's diameter for near spherical particles. An asperity for a powder is the same as an asperity for a homogeneous material. The important point is that an asperity for a powder may consist of a portion of, one, or more particles.

For the purpose of discussing reflectance of rough materials it is necessary to define properties of the surface which aid in classifying theories. The most widely used properties are the root-mean-square height σ_0, peak to valley height σ, and the ratio of these to the wavelength. Also, for statistical analysis an autocorrelation parameter of the surface height distribution which is a measure of the distance between asperties is used.

Shadowing, multiple scattering and polarization of the light by the rough surface are phenomena which are difficult to include in analytical predictions. Figure 2a shows the multiple scattering of wave A and B and the shadowing of facet E by facet D. The multiple scattering is much more unwieldy for powder samples (Figure 2b) because many interfaces below the surface of the powder cause scattering in all directions.

In the analysis of reflection from rough surfaces electromagnetic theory may be applied to the entire surface or each facet may be treated as a plane reflector. The second treatment is called geometric analysis even though the reflection of each mirror may be obtained from electromagnetic theory. In the geometric analysis diffraction and interference effects are assumed to be small so the problem is to determine in what direction each mirror facet reflects the incident

energy. In any case a familiarity with electromagnetic theory is necessary to appreciate the problems of reflection from rough surfaces. A summary of this theory for reflection is presented below.

As with any science, Electromagnetic Theory is based upon experimental laws and equations, For a resistor, capacitor and inductor, the governing equations are

$$I = GV, \quad Q = CV, \quad V = L\frac{dI}{dt}. \tag{6}$$

Where

C =capacitance,

G =conductance,

t =time,

I =current,

L =inductance,

Q =charge,

V =electromotive force.

When these equations are generalized to the electromotive field, the following equations are obtained for resistive, capacitive and inductive fields:

$$\overline{J} = \sigma\overline{E}, \quad \overline{D} = \epsilon\overline{E}, \quad \overline{B} = \mu\overline{H}. \tag{7}$$

The coefficients are related to the electrical circuit quantities;

$$\sigma \sim G, \quad \epsilon \sim C, \quad \mu \sim L. \tag{8}$$

Where

$\overline{B}$ =magnetic flux density,

$\overline{D}$ =electric flux density,

$\overline{E}$ =electric field,

$\overline{H}$ =magnetic field,

$\overline{J}$ =current vector,

ϵ =permittivity,

μ_1 =permeability,

σ_1 =conductivity.

The governing laws are:

1. Conservation of charge, which leads to the equation of continuity

$$\text{div } \overline{J} = -\frac{\partial q_v}{\partial t}, \quad q_v = \lim_{\Delta t \to 0} \frac{Q}{\Delta t} \tag{9}$$

2. Gauss's theorem

$$\oint_S \overline{D} \cdot d\overline{S} = Q, \tag{10}$$

where S is a closed surface. This leads to

$$\text{div } \overline{D} = q_v \tag{11}$$

3. Ampere's Law

$$\oint \overline{H} \cdot d\overline{l} = I \tag{12}$$

which leads to

$$\text{CURL } \overline{H} = \overline{J} \tag{13}$$

4. Faraday's Law, which leads to

$$-\text{ CURL } \overline{E} = \frac{\partial \overline{B}}{\partial t} \tag{14}$$

These laws can be used to obtain the Maxwell Equations. They are

$$-\text{ CURL } \overline{E} = \frac{\partial \overline{B}}{\partial t}, \quad \text{CURL } \overline{H} = \frac{\partial \overline{D}}{\partial t} + \overline{J}, \tag{15}$$

$$\text{div } \overline{D} = q_v, \text{ and div } \overline{B} = 0 \tag{16}$$

which along with the continuity equation

$$\text{div } \overline{J} = - \frac{\partial q_v}{\partial t} \tag{17}$$

and the constitutive equations

$$\overline{J} = \sigma_1 \overline{E}, \quad \overline{D} = \varepsilon \overline{E}, \quad \overline{B} = \mu_1 \overline{H} \tag{18}$$

are used to determine the vector field containing the vectors $\overline{B}$, $\overline{D}$, $\overline{E}$, $\overline{H}$, $\overline{J}$, and the scalar q_v. Among the equations above, only six are independent. The boundary conditions for reflection are:

1. The normal component of $\overline{B}$ at a boundary is continous;
2. $\overline{E}$ parallel to the surface must be continous;
3. $\overline{H}$ parallel to the surface must be continous;
4. $\overline{D}$ normal to the surface must be continous.

By suitable manipulations the Maxwell equations can be transformed into wave equations for reflection from surfaces (9);

$$\nabla^2 \overline{E} - \text{grad div } \overline{E} = \mu_1 \sigma_1 \frac{\partial \overline{E}}{\partial t} + \varepsilon \mu_1 \frac{\partial^2 \overline{E}}{\partial t} \tag{19}$$

and

$$\nabla^2 \overline{H} = \mu_1 \sigma_1 \frac{\partial \overline{H}}{\partial t} + \mu_1 \varepsilon \frac{\partial^2 H}{\partial t} \tag{20}$$

For electrical conductors and nonconductors the solution is the form

$$E_y = E_{yo} \exp\{2\pi j \nu t - \Gamma x\} \tag{21}$$

where Γ is called the propagation coefficient and is given by

$$\Gamma = \frac{2\pi \nu j}{c_o}(n - jk) \qquad \text{for conductors} \tag{22}$$

and

$$\Gamma = \frac{2\pi \nu j}{c} \qquad \text{for nonconductors.} \tag{23}$$

A similar solution is obtained for $\overline{H}$.

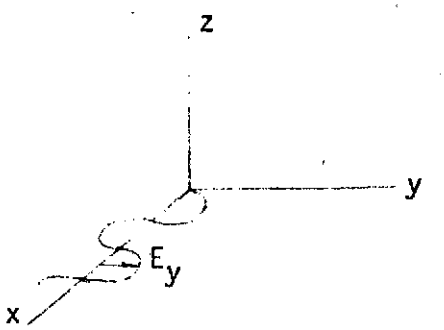

Figure 3. Coordinate System for Electromagnetic Theory

The coordinate system in Figure 3 shows the electric wave which is said to be plane polarized in the xy plane. The complete solution is given by E_y and E_z. For analytical studies involving reflection, the vectors are taken perpendicular and parallel to the plane of incidence. The plane of incidence is the plane containing the incident ray and the normal to the surface, called the P-plane. The S-plane contains the incident ray and is perpendicular to the P-plane.

Generally it is found that the reflectance is a function of the vector under consideration and thus the two vectors may not be reflected with the same magnitude. Also, the reflected energy may not have the same polarization as the incident energy, where polarization can be taken as the ratio of the two light vectors. For rough surfaces this depolarization of the incident energy is due to diffraction by the surface facets.

Using the solution for the electric vectors and the boundary conditions the reflectance coefficient for the interface between two dielectrics can be obtained. The equations called Fresnel's Equations are

$$R_p = \frac{E_r}{E_i}\Big)_p = \frac{n_2\cos(\theta) - n\cos(\theta_2)}{n_2\cos(\theta) + n\cos(\theta_2)}, \tag{24}$$

$$R_s = \frac{E_r}{E_i}\Big)_s = \frac{n\cos(\theta) - n_2\cos(\theta_2)}{n\cos(\theta) + n_2\cos(\theta_2)} \tag{25}$$

n and n_2 are the refractive indices of medium 1 and 2 respectively which are related by Snell's equations,

$$\theta = \theta_2, \quad n\sin(\theta) = n_2\sin(\theta_2) \tag{26}$$

The geometry is shown is Figure 1. The power reflectance is given by

$$\rho_s = R_s^2, \quad \rho_p = R_p^2 \tag{27}$$

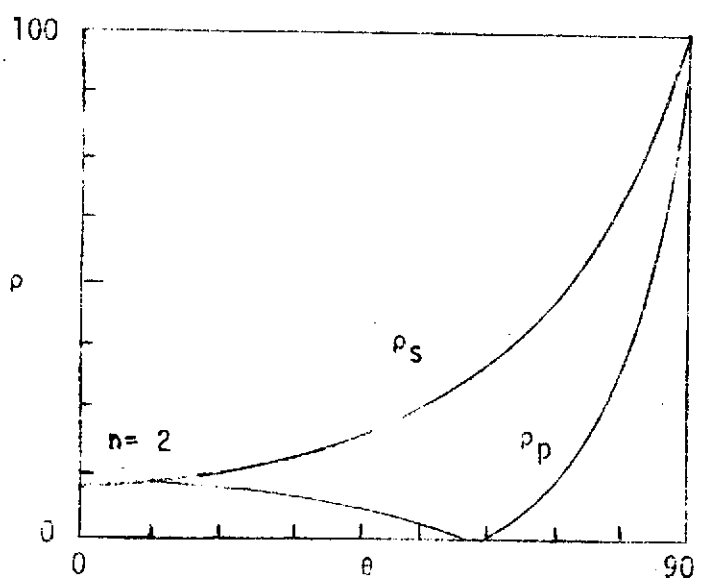

Figure 4. Specular Reflection of Nonconductor

As shown in Figure 4 ρ_s and ρ_p are not equal. This is one of the most important phenomenon in the theory of reflection from dielectrics. The angle for which ρ_p is a minimum is called the Brewster angle.

Reflection from Rough Homogeneous Materials

Theories of reflection from rough surfaces are classified by using the ratio σ_0/λ . Based on this ratio the following classification can be considered: (a)$\sigma_0/\lambda \sim 1$, physical optics are applicable, (b)$\sigma_0/\lambda >> 1$, geometrical optics are applicable, (c)$\sigma_0/\lambda << 1$, the reflectance is specular. For the physical optics regime electromagnetic theory is used. The physical optics solutions are called Kirchhoff's and Rayleigh's method. In the Kirchhoff method the wave equation is put in the form of an integral, called Helmholtz integral, by use of the divergence theorem and Green's First and Second Theorems (19). The boundary conditions are then approximated to allow solutions for specific problems. The usual boundary conditions on a facet of the rough surface are taken as the electric field on a plane reflector. For a randomly rough surface a solution can be obtained under some fairly restrictive conditions.

The most widely used results which are obtained from the Kirchhoff's method is that due to Davies (24). The restrictions being; (1) surfaces which are perfect conductors,

(2) surfaces which are slightly rough, and (3) surfaces which are very rough. The results of Davies are summarized below:

$$\rho_{I,s}(\theta) = \rho_0 \exp\{-(4\pi\sigma_0 \cos\theta/\lambda)^2, \quad \sigma_0/a \ll 1 \tag{28}$$

$$\rho_{I,d}(\psi,\zeta;\theta,\phi) = \frac{\pi^3 a^2 \rho_0^2}{\lambda^4}(\cos\psi + \cos\theta)^4 \rho_0 \exp\left\{-\left(\frac{\pi a}{\lambda}\right)^2 \left[\sin^2\psi + \sin^2\theta - 2\sin\psi \sin\theta \cos(\phi - \zeta)\right]\right\} \tag{29}$$

$\rho_0/a \ll 1, \ \rho_0/\lambda \ll 1$

$$\rho_{I,d}(\psi,\zeta;\theta,\phi) = \frac{(a/\sigma_0)^2}{32\pi}(\cos\theta + \cos\psi)^2 \rho_0 \exp\left\{-(a/\sigma_0)^2 \cdot \left[\frac{\sin^2\psi + \sin^2\theta - 2\sin\psi \sin\theta \cos(\zeta - \phi)}{(\cos\psi + \cos\theta)}\right]\right\} \tag{30}$$

$\sigma_0/a \ll 1, \quad \sigma_0/\lambda \gg 1$

A very important point is that the Davies solution is in closed form and contains two terms which are a diffuse reflectance term and a specular reflectance term. In order to use the results of Davies as a pure predictive method it is necessary to obtain a statistical model of the surface. The two values needed are a height or roughness parameter and a correlation parameter. No references were found in the literature where the correlation parameter was calculated or measured. Instead the Davies solution is fitted to

experimental data.

Nevertheless, Beckmann (19) who obtained results similar to Davies and explains the derivations in detail, discussed some important results of this theory. These are: (1) as the correlation parameter increases, the surface reflectance is more specular; (2) as the surface roughness decreases, the reflection becomes more specular; and (3) as the wavelength increases, the surface reflects more specular. It is important to note that the specular component is not said to be due to subsurfaces which are parallel to the mean surface. This hypotheses is used to explain the specular component of compressed powder specimens, Kortum (8).

In the Rayleigh method the reflected field is assumed to be an infinite series with unknown coefficients which are computed by using the boundary conditions. This procedure results in a set of infinite linear equations for the coefficients. The mathematical difficulties of this method prohibit solutions to all but slightly rough surfaces. Another factor which makes this method unappealing is that results cannot be put in closed form.

When $\sigma_0/\lambda >> 1$, geometrical optics are used to explain diffuse reflection. Smith and Hering (42) have used geometrical optics to determine the bidirectional reflectance of a surface composed of V shaped elements. Each element is

assumed to have a reflectance factor which is a function of the element's included angle and direction of incident energy. The elements are oriented according to a distribution function which determines the reflectance of the elements in any detector direction. The reflectance for the surface is the sum of the reflectance for all the elements. From the result presented by Smith and Hering it would seem that geometrical optics cannot be used to explain diffuse reflection at large angles of incidence. This is in agreement with Kortum's (8) review of works using an elementary mirror hypotheses for diffuse reflection. Voishville (47) used geometrical optics in a similar analysis as Smith and Hering to explain the large forward scatter from a rough glass specimen. Look and Love (32) were able to fit a Monte Carlo Geometrical optics method to data by using a roundness parameter in addition to the usual two surface parameters.

Survey of Experimental Papers

It is evident from the theoretical discussion that a large number of variables are involved in the investigation of the bidirectional reflectance. This and the fact that a complete determination of the reflectance involves many wavelengths and angles have caused most investigators to present minimal data. The intent of most investigators

appears to be to give data that indicate characteristics and phenomena and to emphasize correlation of the data. For the most part, attempts are made to correlate data with the results of Davies (24) who obtained a closed form analytical solution for a random conducting surface by employing the Kirchhoff method. In order to use this method for prediction and correlation, it is necessary to experimentally determine two statistical quantities, the rms roughness and a correlation parameter for the roughness.

Torrance (44) discusses two experimental problems involved in measuring the bidirectional reflectance. The first is due to the limited range of operation of most detectors. Detectors measure energy at a certain level which vary several orders of magnitudes and the difference between the incident energy and reflected energy is much larger than the operating range of most detectors. To get around this problem, most investigators present their results as a relative reflectance. This is the reflectance in any direction divided by the reflectance in the specular direction or some other reference direction.

The second factor is the stray light reaching the detector. In the system Torrance used, the detection system could not differentiate between the stray light signal and that portion of the signal due to the reflection from the specimen. For this reason it was necessary to obtain a stray

light signal for all directions to be investigated, which was then subtracted from the reflectance measurements.

Table 1 is a selected summary of bidirectional reflectance data presented in the literature. The first publication to give bidirectional reflectance data is Eckert (25). As with Munch (36) and Middleton (34), his investigation is not for monochromatic incident energy. Nevertheless, the reflectance behavior of some important engineering materials are given. The data of Torrance (44) and many other investigators show two trends; with decreasing wavelength the reflectance of a given surface approaches that of an ideal diffuse reflector, with increasing wavelength the reflectance approaches that of an ideal specular reflector. Another trend of importance discussed by Torrance (45) is off specular peaks in the bidirectional reflectance data. Torrance's data shows that it is possible to have the maximum reflectance in an angle other than the specular angle.

Bidirectional reflectance data presented in the literature also show that reflectance can frequently be divided into a specular and a diffuse component. The diffuse component may be close to lambert over a wide range of conditions and the specular component may change considerably in magnitude.

TABLE 1

TABULATION OF SELECTED REFERENCES

AUTHOR	WAVELENGTH OF SOURCE	ANGLES, DEGREES	MATERIALS
Eckert (1936) (25)*	Blackbody	ψ = 0 θ = 0-180 ϕ = 0, 180 ζ = 180	Various engineering surfaces
Munch (1955) (36)	Blackbody 355-995	ψ = 0, 15, 30, 45, 60 θ = 0, 90 ϕ = 0, 180 ζ = 180	White typewriter paper, black oxidized brass, white pine, colorsted anodically oxidized anticorodal sheet sandblasted anticorodal sheet
Middleton and Mungall (1952) (34)	Visible	ψ = 0, 30, 45, 60, 75 θ = 0-80 ϕ = 0, 180 ζ = 180	Snow
Torrance and Sparrow (1965) (44)	0.5 - 12μ	ψ = 10, 45 θ = 0-70 ϕ = 0, 45, 90, 180 ζ = 180	Fused polycrystalline magnesium oxide ceramic
Birkebak and Eckert (1965) (20)	2 - 10μ	ψ = 10 θ = 0-70 ϕ = 0, 45, 90, 135, 180 ζ = 180	Ground glass coated with aluminum, nickel
Torrance and Sparrow (1966) (45)	0.5 - 5μ	ψ = 10, 20, 30, 45, 60, 75 θ = 0-85 ϕ = 0, 180 ζ = 180	Aluminum, nickel, copper, nickel copper alloy, magnesium oxide ceramic

*Refers to reference in the bibliography.

TABLE 1 CONT.

AUTHOR	WAVELENGTH OF SOURCE	ANGLES, DEGREES	MATERIALS
Herold and Edwards (1966) (27)	2.5, 5.0, 7.5μ	ψ = 0, 20, 40, 60 θ = 0-80 ϕ = 0-180 ζ = 180	Sintered-bronze, glass-beaded projection screen, sand blasted aluminum, 100 mesh wire-screen bonded to mylar, all coated with either aluminum or gold
Oetking (1966) (39)	75 watt zenon arc lamp	ψ = 0 θ = 0-40 ϕ = 0, 180 ζ = 180	MgO, Al_2O_3(no. 80-800grit), several basic rocks and unconsolidated samples
Brandenberg and Neu (1966) (21)	0.507, 0.533μ	ψ = 15-75 θ = 15, 30, 45, 60, 75 ϕ = 0, 150 ζ = 180	MgO coating, barium sulfate paint, zinc oxide paint, aluminum
Miller and Kannon (1967) (35)	0.546, 2.0μ	ψ = 0, 30, 60 θ = 0-60 ϕ = 0, 180 ζ = 180	MgO
Love and Francis (1967) (33)	0.6 -10.0μ	ψ = 10, 30, 60 θ = 0-90 ϕ = 0 ζ = 180	Type 302 stainless steel

TABLE 1 CONT.

AUTHOR	WAVELENGTH OF SOURCE	ANGLES, DEGREES	MATERIALS
Smith, Tempelmeyer, Muller and Wood (1969) (41)	0.9μ	ψ = 10, 30, 50, 70 θ = 0-85 ϕ = 0-60, 180 ζ = 180	CO_2 cryodeposits on polished copper and black epoxy paint surfaces
Loehrlein, Winter and Visicanta (1970) (31)	0.43, 0.55μ	ψ = 30, 45, 60 θ = 0-85 ϕ = 0, 30, 60 ζ = 90, 180	Aluminum, polycrystalline magnesium oxide, projection screen, well characterized V-grove
Zentner, MacGregor and Pogson (1971) (49)	0.5, 2.0, 5.0, 10, 15μ	ψ = 0-75 θ = 0-85 ϕ = 0-180 ζ = 180	MgO, gold sandpaper(150-400 grit)

Statement of Research Problem

The objective of this investigation was to experimentally study the bidirectional reflectance of zinc oxide (SP500) in the spectrum 0.250 to 2.500 microns and the hemisphere above the specimen. The independent variables for the investigation are wavelength, source zenith and azimuth angles, detector zenith and azimuth angles, and polarization. To meet the objectives a system using state of the art components was designed and assembled by the author.

CHAPTER II

EXPERIMENTAL APPARATUS AND PROCEDURES

Experimental Apparatus

The system used to measure the bidirectional reflectance is shown in Figures 5, 6, and 7. The subsystems are the monochromator, light sources, exit optics, bidirectional device, and the detection system.

The monochromatic source consists of a Bausch and Lomb 500mm grating monochromator with Bausch and Lomb tunsgten ribbon and deuterium lamps. The spectral response of the monochromator source system is shown in Figures 10, 11, and 12. The data presented in Figure 12 was measured with the subject apparatus using a lead sulfide detector. The monochromator has stray light of less than 0.1 per cent at 0.300 microns, wavelengths can be set directly to 0.001 microns and the slits can be set directly to 0.01mm. An Ealing mercury calibration lamp was used to check the wavelength accuracy of the monochromator. The result shown in Table 2 demonstrates that wavelengths can be set to within 0.001 microns.

In order to obtain the maximum energy from the monochromator three gratings was used. For the wavelength

range 0.25 to 0.45 microns a 600 grooves/mm grating blazed at 0.300 microns was used. Between 0.45 and 1.4 microns a 600 grooves/mm grating blazed at 0.75 microns was used. To obtain energy out to 2.5 microns a 300 grooves/mm grating blazed at 2.00 microns was used. The 600 grooves/mm gratings gave a 3.3 nm/mm slitwidth first order dispersion. A dispersion of 6.6 nm/mm was obtained with the 300 grooves/mm grating. The first order bandwidth is the dispersion times the slidwidth.

With this optical arrangement higher order wavelengths would be present but are eliminated with Corning # 4-97 color filter for the range 0.360 to 0.620 microns, Corning # 2-58 for the range 0.640-1.100 microns, and a Corning # 7-56 color filter for the range 1.100 to 1.400 microns. For the spectrum between 1.4 and 2.5 microns a Spectrum Systems interference filter was used to eliminate higher orders. The transmission characteristics for these filters in the spectrum in which they are used are shown in figure 13.

A bidirectional device was used to vary independently the incident zenith and azimuth angles, and the reflected zenith and azimuth angles. This device is shown in Figure 8 and schematically in Figure 9. Ideally the center of the specimen should have zero movement and the distance from the detector to the specimen should not change for changes in the detector or source zenith. For the bidirectional device used

in this study the movement of the center of the specimen for a 90 degree change in source zenith is 0.1 mm and the movement of axis x" off center for a 90 degree change in source zenith is 0.1 mm. The instrument was aligned by placing a front surface mirror on the specimen holder and adjusting the angles until the light was reflected back into the monochromator, thus locating the normal direction. The bidirectional device was shielded from the exit optics and the monochromator to prevent chopped light from striking the detectors directly.

Referring to Figures 8 and 9, the coordinate system was fixed on the specimen and the source and arms C were fixed relative to earth. The zero for the detector and source azimuth was in the specular plane and 180 degrees from the incident energy. The zero for the source and detector zenith was normal to the specimen. Knob E was used to set the source azimuth and can be rotated about the y-axis without moving any other part of the device. Arm A was used to set the detector azimuth and can be rotated about the y-axis. Arm B was used to set the source zenith and can be rotated about the x'-axis and Arm C was used to set the detector zenith. All angles can be changed independently.

A schematic of the detection system is shown in Figure 14. The detectors are Infrared Industries ambient lead

sulfide and RCA 1P28A photomultiplier which are operated at ambient temperature. The linearity of the PMT was checked at 0.550 microns with precision neutral density filters obtained from Special Optics and is shown in Figure 15. Table 3 which is reflectance data of ZnO at 0.7 microns shows both detectors give essentially the same results. The PbS gives a smaller specular component because the solid angle is larger than that of the PMT and the specular component has a small solid angle. For all other data the detectors have the same solid angle. The detectors are mounted on arm D such that they are over illuminated (all of the detector sensitive area is used) allowing direct measurements of the reflected energy to be made. A shield recommended by RCA was used with the PMT to eliminate effects of magnetic fields. The shield (P-13P32V1) was obtained from the Perfection Mica Company. Twelve RCA VS146 mercury batteries supply the bias voltage for the lead sulfide detector and the photomultiplier voltage was regulated by a Hewlett Packard model 6515A power supply which has line regulation of 0.01% or 16 mV.

Polarizers can be mounted near the filter and in front of the detector to study polarization. Polaroid type HNP'B ultra violet polarizers are used for the range 0.25 to 0.90 microns and Polaroid type HR infrared polarizers are used for

the spectrum 0.90 to 2.5 microns. The spectral response of the polarizers are shown in Figure 16. The use of data taken with polarizers are discussed in Appendix A. The polarizers were aligned by use of the brewster angle of a glass plate. At a source zenith of about 60 degrees the reflected energy from a glass plate is a minimum for energy polarized in a plane containing the incident ray and the reflected ray. For this same source zenith when the polarizer is rotated 90 degrees a maximum is obtained.

A model 391A lock-in amplifier, manufactured by the Ithaco Company, was used to measure the detector signal. The amplifier can measure a signal from 0.1 microvolts to 1 volt full scale provided a reference signal of the same frequency is available. The important features of the amplifier are; a time constant range from 0.175 ms to 125 sec which corresponds to a noise bandwidth of 0.01 Hz to 0.001 Hz, three sensitivity modes which allow a trade off between output stability and the capability of the amplifier to measure a signal that has noise, and a zero depress. The combination of these allow a trade off between output signal fluctuation due to noise, output drift, time to take a reading, and readout accuracy. The instrument has a calculated accuracy of 1% and a nonlinearity of 0.05%.

The detection system was designed so that the limiting

minimum detectable signal was determined by the PMT and PbS. The amplifier noise was less than 0.25 microvolts at 666 Hz, the PbS noise was approximately 1 microvolt and the photomultiplier noise was approximately 50 microvolts. The amplifier overloads at a sensitivity setting of 0.300 microvolts when using the Pbs and at 3 microvolts when using the PMT. For the PbS approximately 57% of the runs were with a 30 microvolts sensitivity, 29% with a 10 microvolts senitivity and 14% with a 3 microvolt sensitivity. For the PMT 53% of the runs were with a 10 mv sensitivity, 12.5% with a 0.1 mv sensitivity and the remainder between 0.1 mv and 10 mv sensitivity. A time constant of 4 seconds was used at 0.5 microns and at other wavelengths a time constant of 12 or 40 seconds was used. For most of the data output noise was within $\pm$0.5% but at 1.25, 0.3 and 2.5 microns some data had output noise of $\pm$1%.

The reference signal was provided by a Princeton Applied Research model 125 light chopper. This chopper has two 16-aperture blades on a common shaft which was driven by a synchronous motor. One blade chops the light from the monochromator and the other chops the light from a small bulb. A photo-transistor detects the light from the small bulb and provides the reference signal. The light was chopped at 667 or 333 Hz. A Hewlett Packard model 680 recorder with

accuracy of 0.1% full scale was used for read out.

A Sorensen and Company model 1000S AC voltage regulator supplies stabilized voltage to the lamps and all electronics.

A photograph of the optical system is shown in Figure 7 and a schematic is shown in Figure 17. All mirrors are front surface aluminum with silicon monoxide protective coating which were obtained from Esco Optics. At the exit of the monochromator the effective aperture ratio was f/4.4. The reflected beam of the concave mirror has an aperture ratio of f/12.65. The incident solid angle was then determined by the opening of the iris diaphragm. With the f number of the exit optics fixed, the size of the illuminated area on the specimen was determined by the setting of the exit slit.

A Dana Laboratories model 4700 digital multimeter was used for initial checkout of the detectors and detector bias circuitry.

Testing Procedures and Experimental Parameters

In the first part of this chapter the experimental apparatus was discussed. In this section additional information concerning the experimental procedures and parameters are discussed.

In the definition of the bidirectional reflectance an

incident beam with a solid angle $d\omega$ is considered. Theoretically this angle should be very small so that variations in the bidirectional reflectance can be properly accounted for. However, the solid angle is related to the f number of the optical system and this is related to the source energy. When the solid angle is decreased the radiant energy incident on the specimen is usually decreased and this results in a decreased signal at the amplifier. To some extent this can be offset by increasing the power to the source, increasing the time constant and decreasing the AC amplification of the amplifier. However, these steps may require a decrease in the stability and an increase in the time to take data. Similar comments apply to the detector solid angle.

The solid angles and other test parameters which are given in Table 4 were set after observing what was used in the literature and after taking preliminary data. The solid angle was made small as possible consistant with the discussion above. The source solid angle was set by stopping the iris diaphragm at an opening of 2.3 cm. The solid angle was computed using the area of the diaphragm opening and the optical distance between the diaphragm and the specimen. In a like manner the distance between the detector and specimen and the detector area are used to

compute the detector solid angle.

The ZnO powder (SP500) which is manufactured by the New Jersey Zinc Company and characteristic particle size distribution were obtained from NASA. The specimen was prepared by weighing 250mg of the powder and pouring it into a recessed specimen holder where it was leveled and compacted with a front surface aluminum mirror. The motion of the mirror was perpendicular to the ZnO surface. The mirror and all other objects used in the preparation of the specimen were first cleaned with denatured alcohol. The diameter of the recess was 2.22cm and the depth was 0.16cm. Other amounts of ZnO and methods of preparation were tried but due to difficulty in duplication of the specimen the above one was chosen. The first method tried was mixing the ZnO with distilled water to form a paste which was applied in the recessed specimen holder. The problem encounted was cracking of the ZnO upon drying. One method tried used an aluminum bar to compact the ZnO. It was discovered that the ZnO would adhere to the bar in an unpredictable manner. Figures 18, 19, 20, and 21 shows photographs of the specimen taken with a scanning electron microscope. At no magnification the specimen looks smooth whereas the photographs show there are crevices ranging in size from about 0.2 to 100 microns. Several other optical

properties of ZnO are given in Appendix B.

For a given test the following were recorded; run number, amplifier sensitivity, filters used, date, time, detector, specimen, wavelength, amplifier zero, amplifier zero offset, and the four angles which determine the direction of the detector and source. The detector signal was measured for detector zenith from 0 to 85 degrees beginning at 0. Then the detector was returned to 0 degrees zenith to obtain a reading for the purpose of determining the drift of the signal. After this, one of the other independent variables was changed and the procedure was repeated. Measurements taken this way for various values of the independant variables were used to compute the relative bidirectional reflectance. The bidirectional data is presented in two ways; the data for any detector azimuth and zenith normalized on the datum at the same azimuth and a zenith of 0 degrees, and as normalized data divided by the cosine of the detector zenith at which the datum was taken.

To determine how the bidirectional reflectance varies with incident angle, data were taken for a detector zenith of 0 degrees while varying the source zenith. The azimuth of both detector and source were fixed for these measurements. These data were normalized on the datum at a source zenith of

10 degrees. Then to compare the reflectance at two different source incident angles the following quantities are formed;

$$\psi^1, \quad \frac{D(\psi^1,180°;\theta,\phi)}{D(\psi^1,180°;0°,0°)} \times \frac{D(\psi^1,180°;0°,0°)}{D(10°,180°;0°,0°)}$$

$$\psi^2, \quad \frac{D(\psi^2,180°;\theta,\phi)}{D(\psi^2,180°;0°,0°)} \times \frac{D(\psi^2,180°;0°,0°)}{D(10°,180°;0°,0°)} \qquad (31)$$

If the comparison is made to check reciprocity each quantity is divided by the cos (θ).

The specular component was measured by obtaining the maximum signal in the specular direction and then checking the detector angle. The specular component for 0.546 microns was calculated from measurements of the specular components using the polarizers by using equation A-4.

The variation of reflectance with wavelength was obtained by measuring the reflected energy for a fixed set of angular variables and the source energy versus wavelength in the polarized P-plane. For the same wavelengths the S-plane energy was also measured for the source and specimen. The ratio of the P-plane ZnO measurement to the source P-plane measurement gives the reflectance variation with wavelength in the P-plane. The S-plane reflectance was computed as follows:

$$D_{s_{ZnO}} = \left(D_p \frac{D_s}{D_p}\right)_{ZnO} \tag{32}$$

$$D_{s_{source}} = \left(D_p \frac{D_s}{D_p}\right)_{source} \tag{33}$$

$$\frac{D_{s_{ZnO}}}{D_{s_{source}}} = \frac{D_{p_{ZnO}}}{D_{p_{source}}} \times \frac{(D_s/D_p)_{ZnO}}{(D_s/D_p)_{source}} \tag{34}$$

Then the total reflectance was computed as the average of the reflectance in the S and P-planes and is designated D_λ. This reflectance is not an absolute value since for the measurements the detector measured only part of the incident energy.

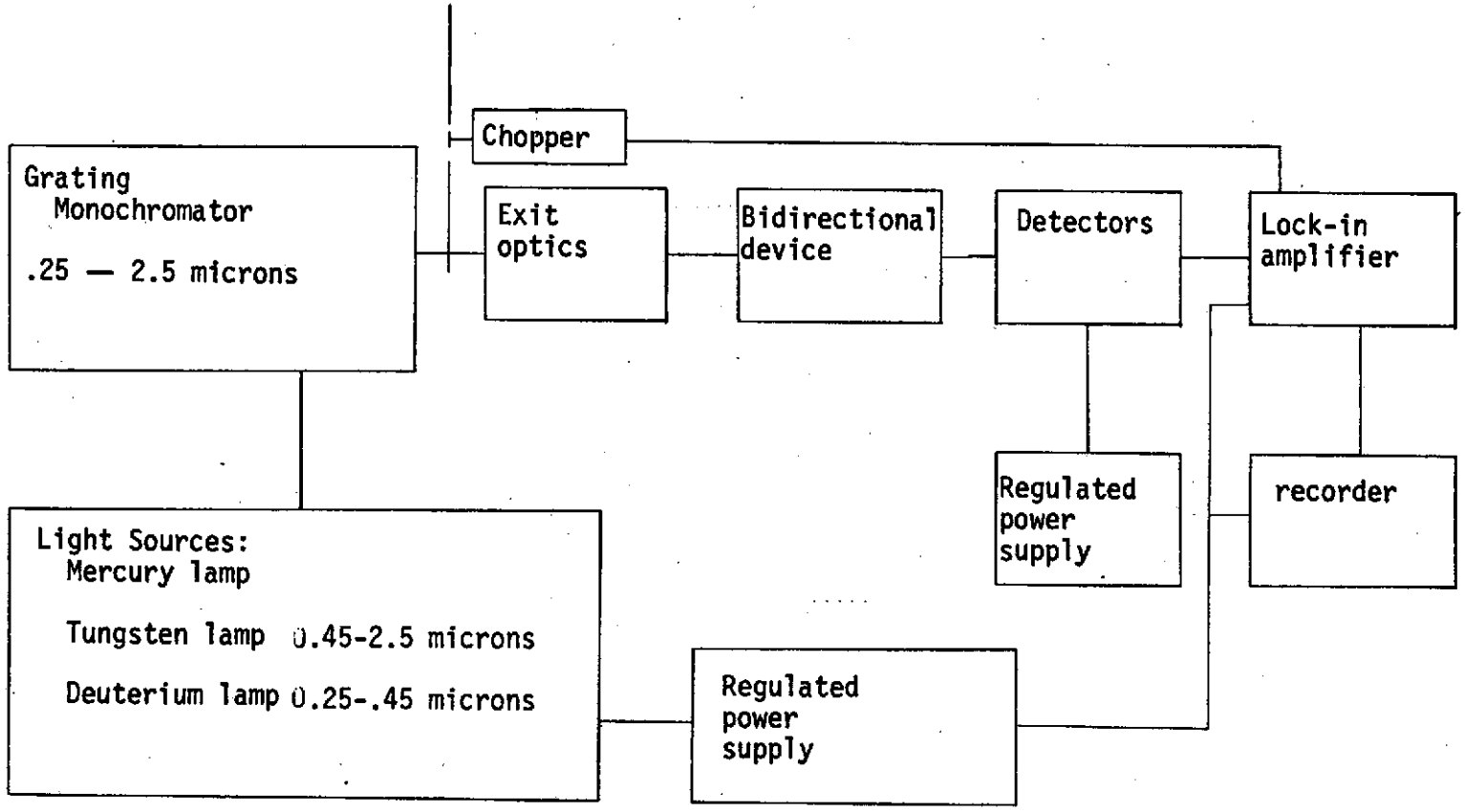

Figure 5. Schematic of Test System

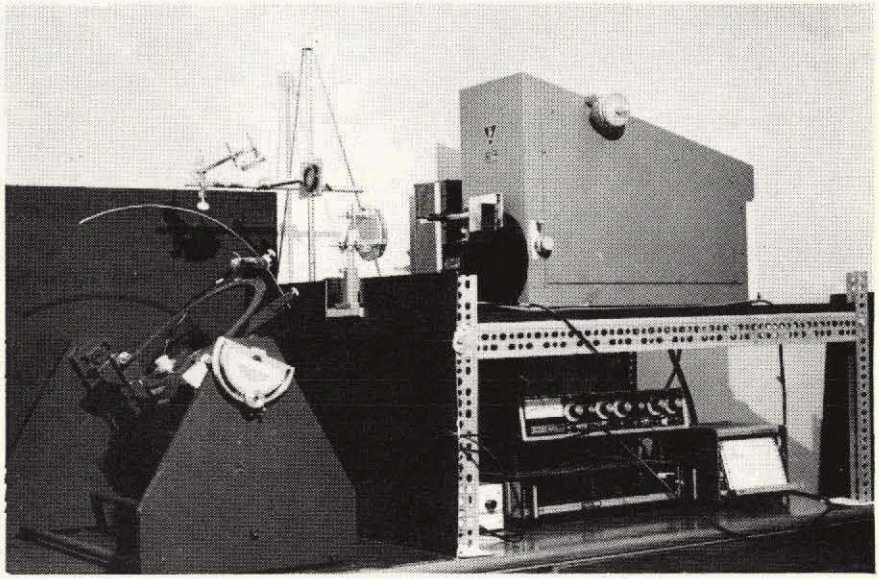

Figure 6. Experimental Apparatus

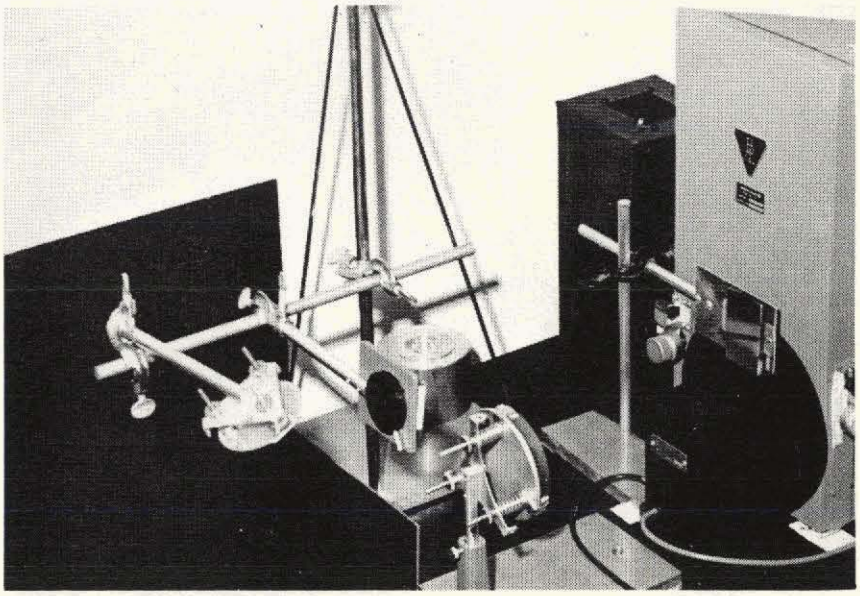

Figure 7. Exit Optics

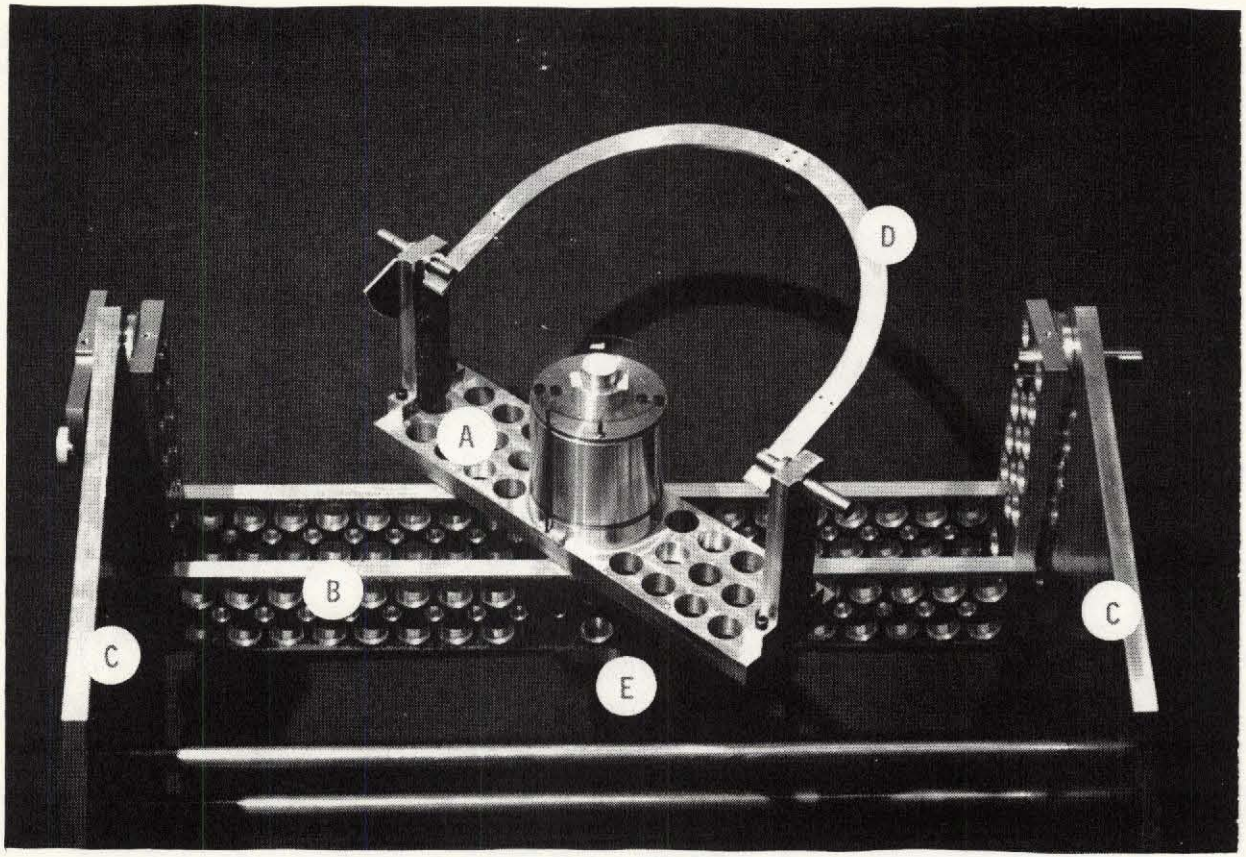

Figure 8. Bidirectional Device

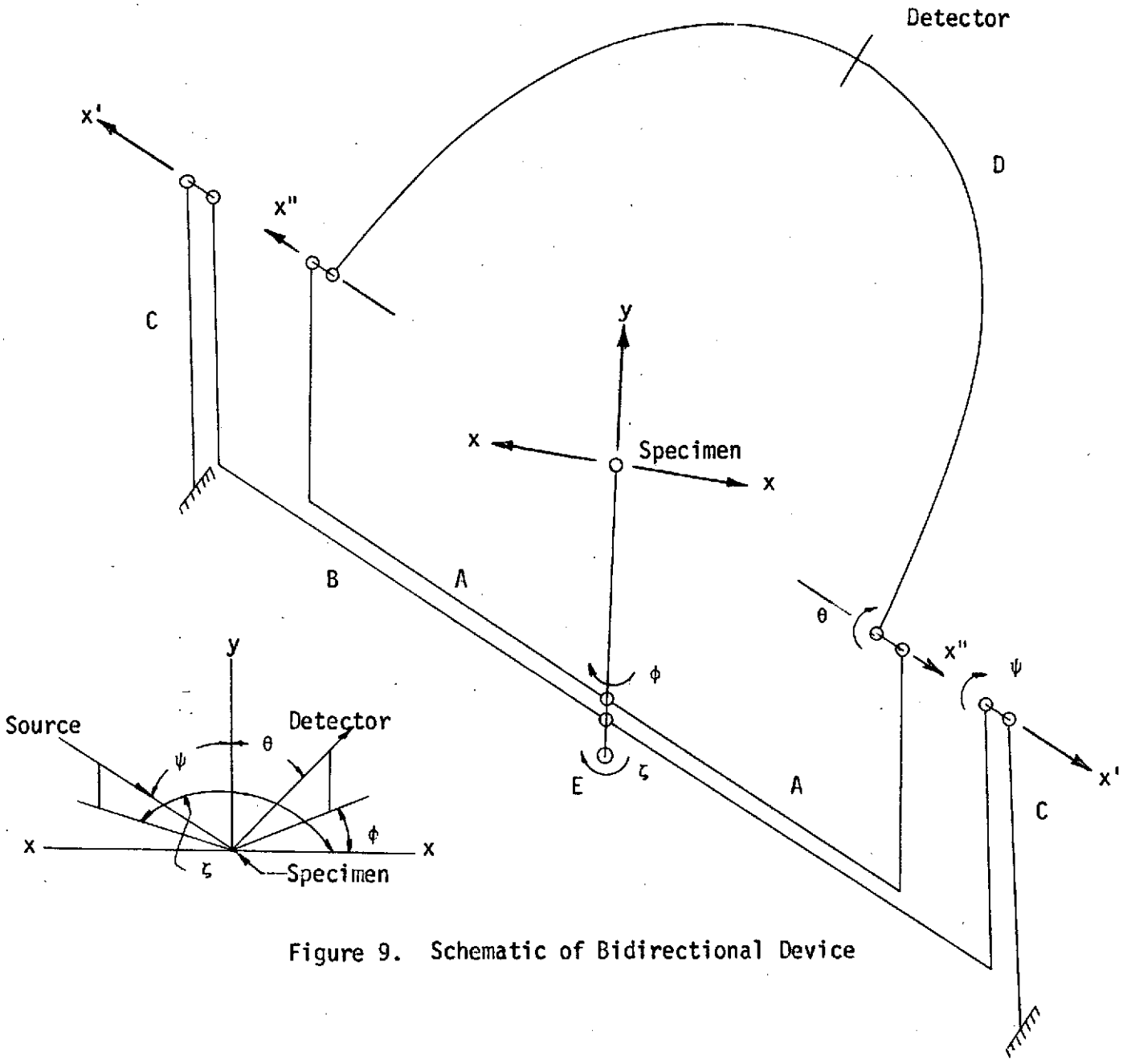

Figure 9. Schematic of Bidirectional Device

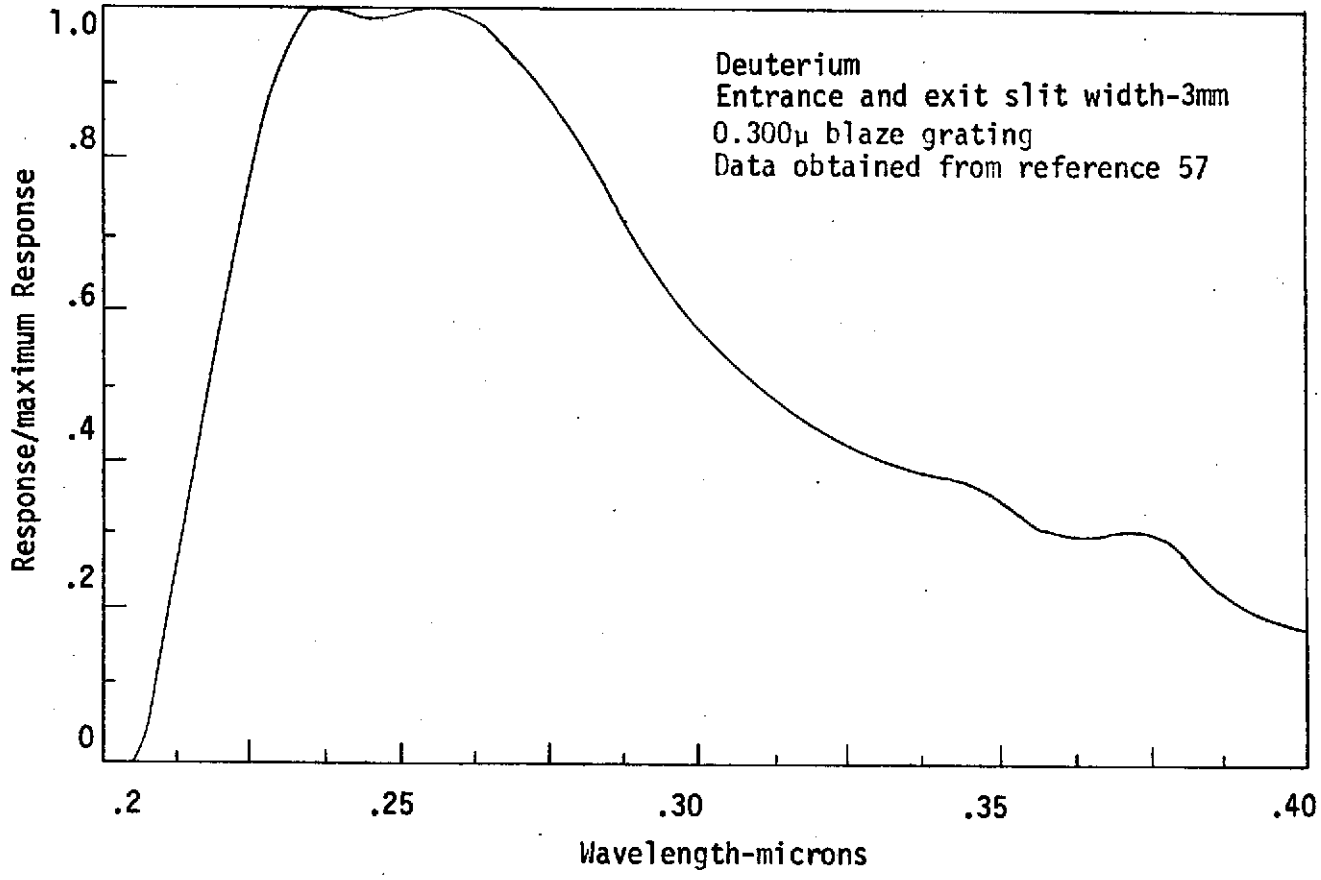

Figure 10. Source Spectral Response

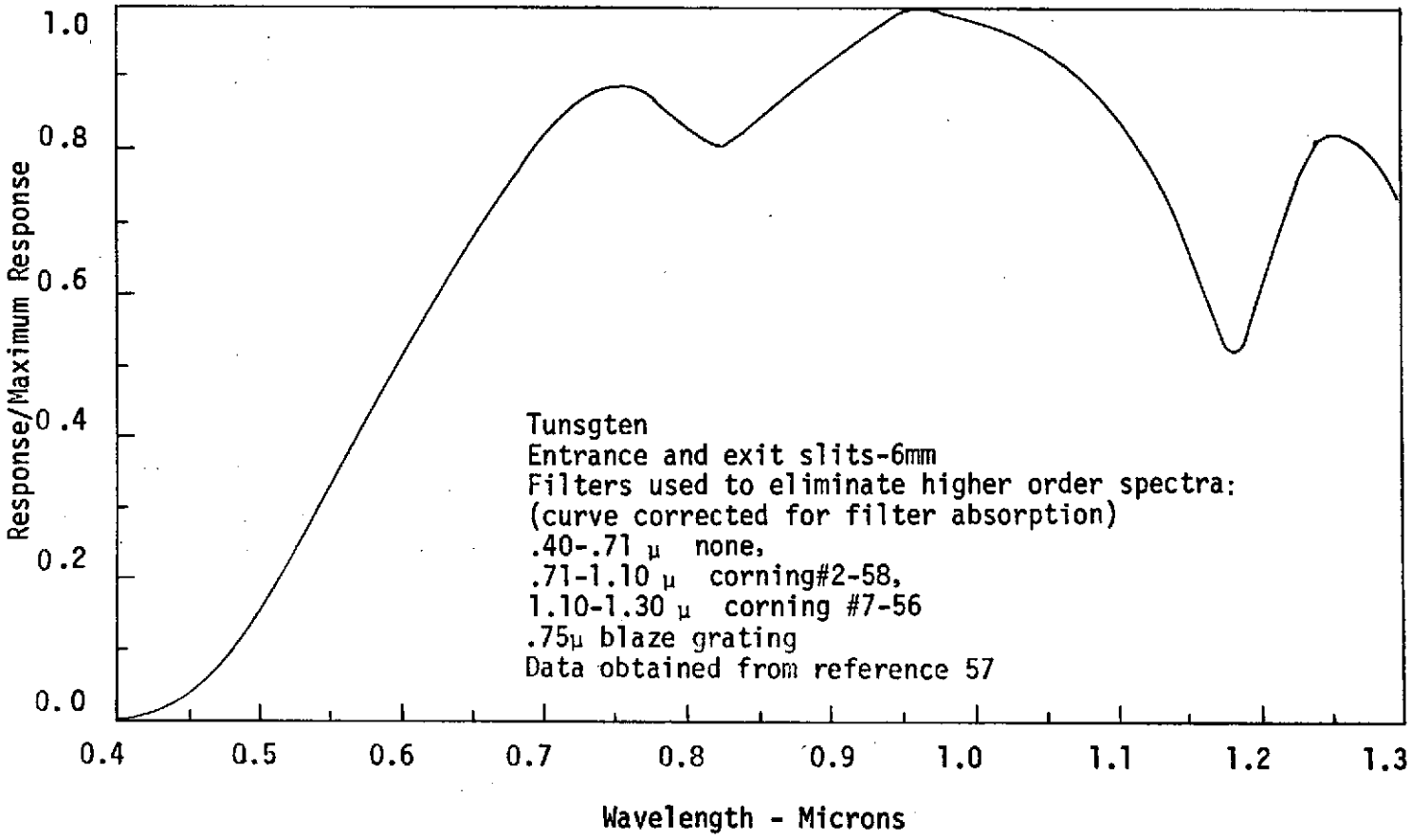

Figure 11. Source Spectral Response

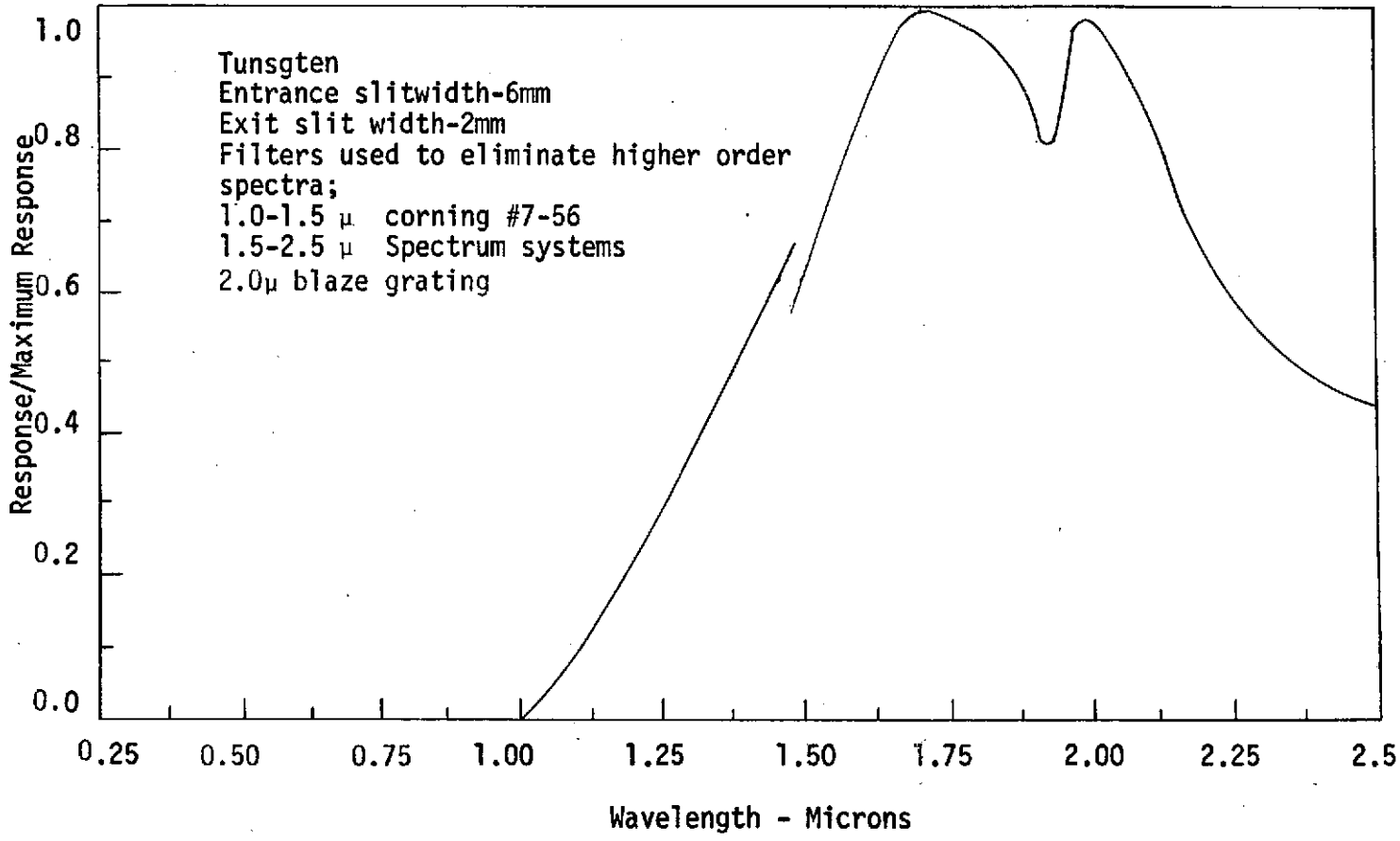

Figure 12. Source Spectral Response

TABLE 2

CHECK OF MONOCHROMATOR CALIBRATION

Monochromator wavelength-μ	Grating	Order used for check*	Hg line-μ**
0.296	0.30 micron blaze	1st	0.2965
0.314		1st	0.3132
0.366		1st	0.3663
			0.3655
			0.3650
0.405		1st	0.4047
0.547		1st	0.5461
0.578		1st	0.5770
			0.5790
0.546	0.75 micron blaze	1st	0.5460
0.625		2nd	0.3126
0.810		2nd	0.4047
1.215		3rd	0.4047
1.160	2.00 micron blaze	2nd	0.5790
1.634		3rd	0.5447
2.316		4th	0.5790

*The monochromator wavelength divided by the order for check gives the measurement of the Hg line.
**Obtained from reference 60.

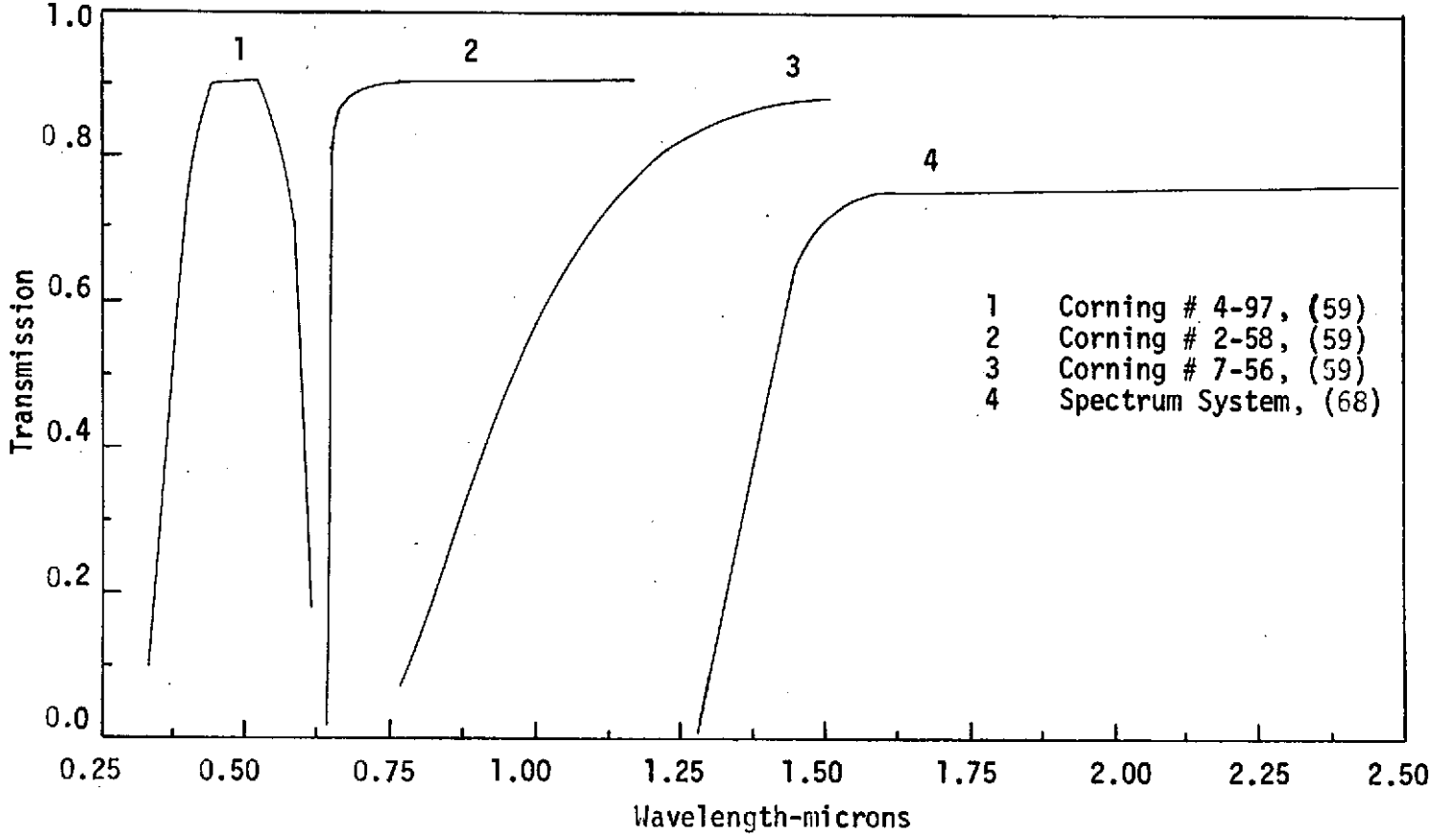

Figure 13. Transmission of Filters

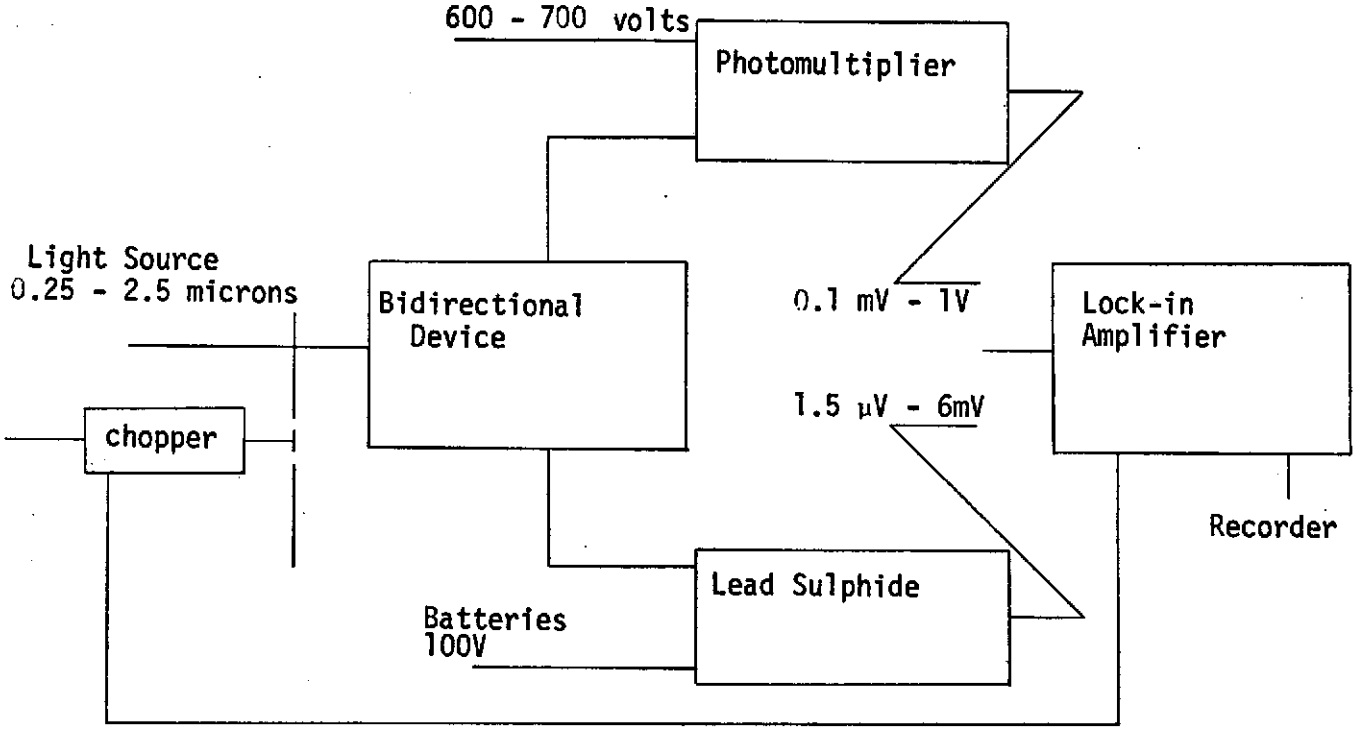

Figure 14. Schematic of Detection System

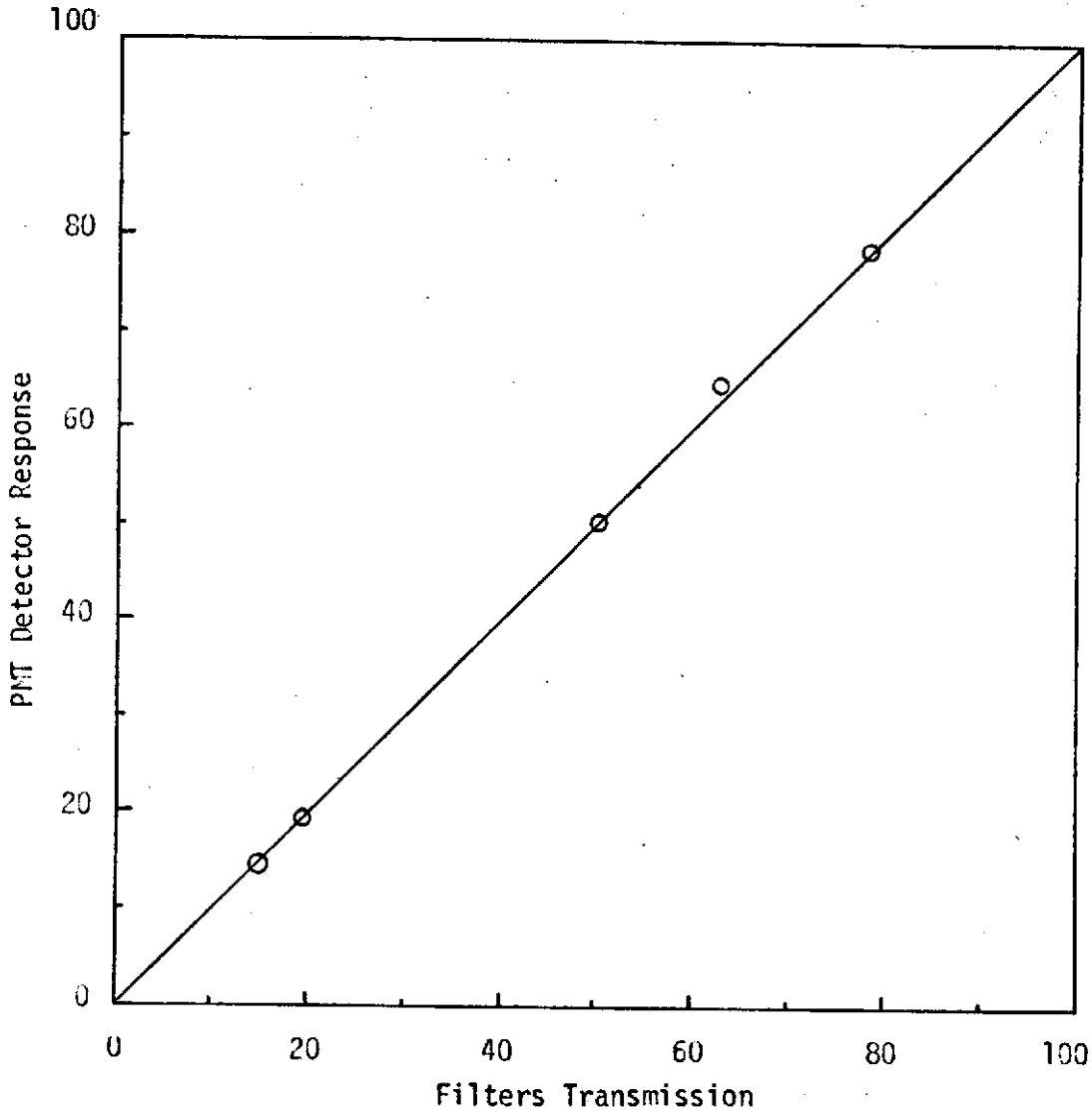

Figure 15. Linearity of PMT

TABLE 3

REFLECTANCE OF ZnO AT 0.700 MICRONS
OBTAINED WITH PMT AND PBS

$D(60,180;\theta,\phi)/D(60,180;0,\phi)$

	PMT		PBS	
θ	ϕ=0	ϕ=180	ϕ=0	ϕ=180
0	1.000	1.000	1.000	1.000
20	0.958	0.939	0.958	0.930
40	0.808	0.784	0.808	0.789
50	0.710	0.707	0.713	0.705
60	2.400	-	1.087	-
70	-	0.373	-	0.388
80	0.234	0.172	0.239	0.183

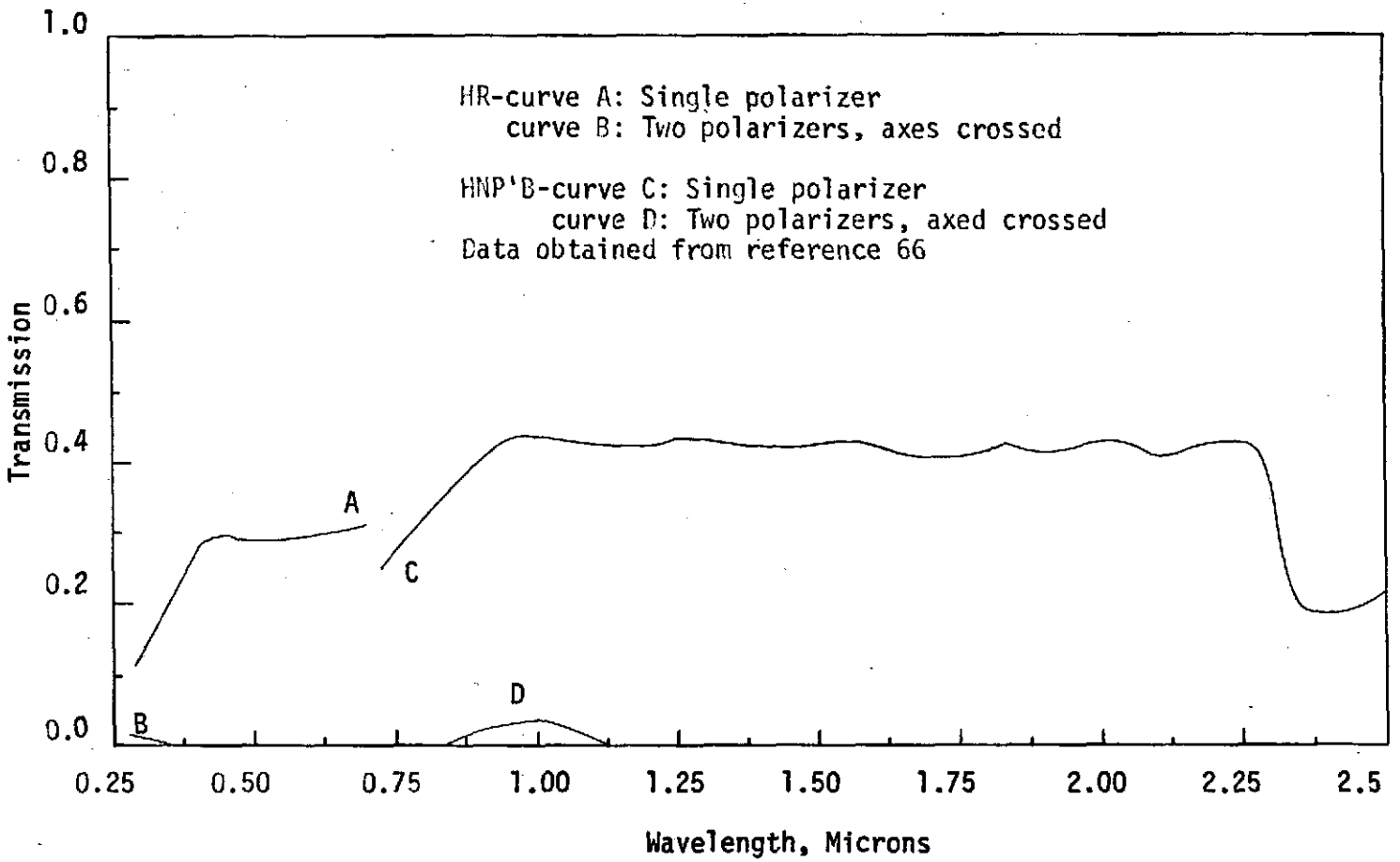

Figure 16. Transmission of Polarizers

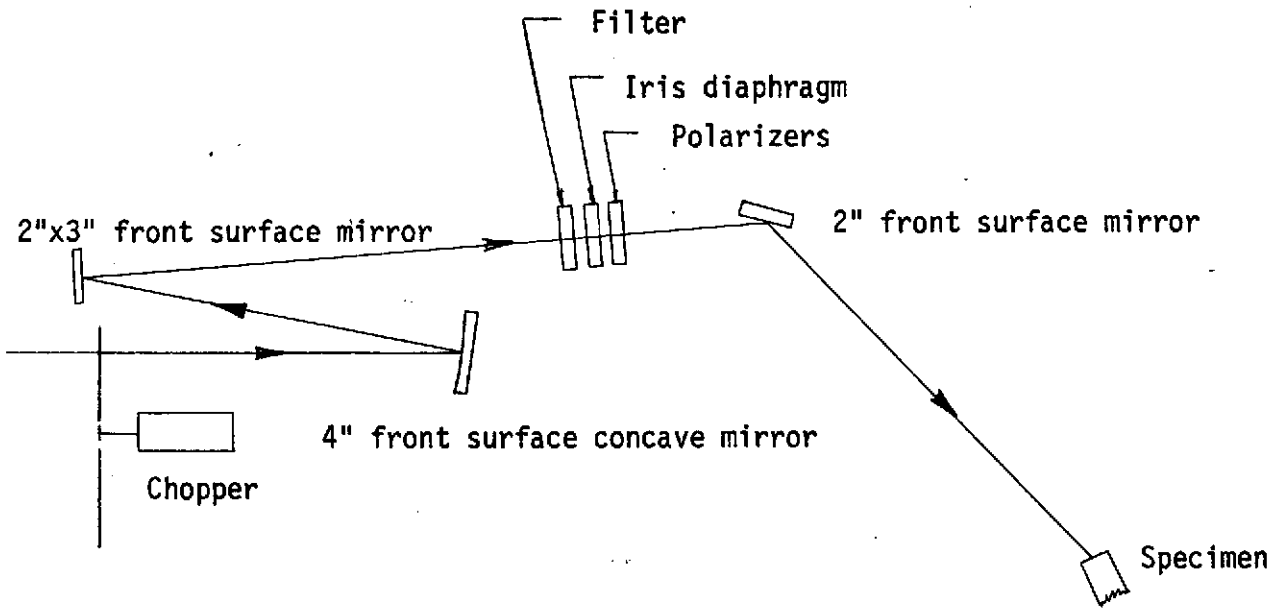

Figure 17. Schematic of Exit Optics

TABLE 4

TEST PARAMETERS AND
SPECIMEN PROPERTIES

Incident energy solid angle	0.00196 steradians
Detector solid angle	0.00076 steradians
Illuminated area on specimen (source zenith of 0°)	1.8x7mm
Bandpass for source wavelength;	
PMT, .25-.75 microns	6.6nm
PbS, .75-2.5 microns	13.2nm
Amplifier output for diffuse data	2-9.7 volts
Amplifier output full scale	0-10 volts
Chopping frequency	333, 666Hz
Time constant	4-40 seconds
Temperature	293.0-300.0 °K
Specimen particle size	0.1-1.0 microns
mean size	0.4 microns

10μ

Figure 18. Photograph of Specimen

4.3μ

Figure 19. Photograph of Specimen

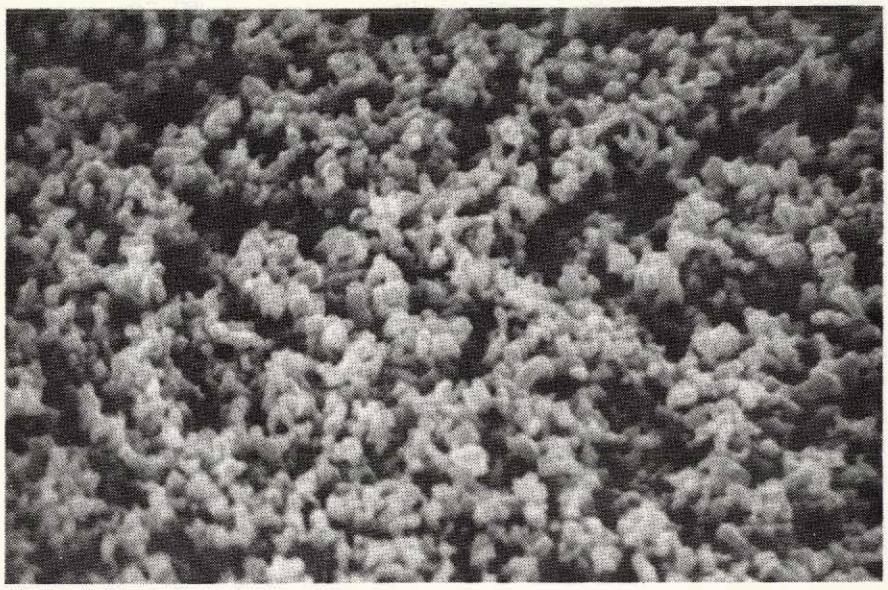

⟷ 1.2μ

Figure 20. Photograph of Specimen

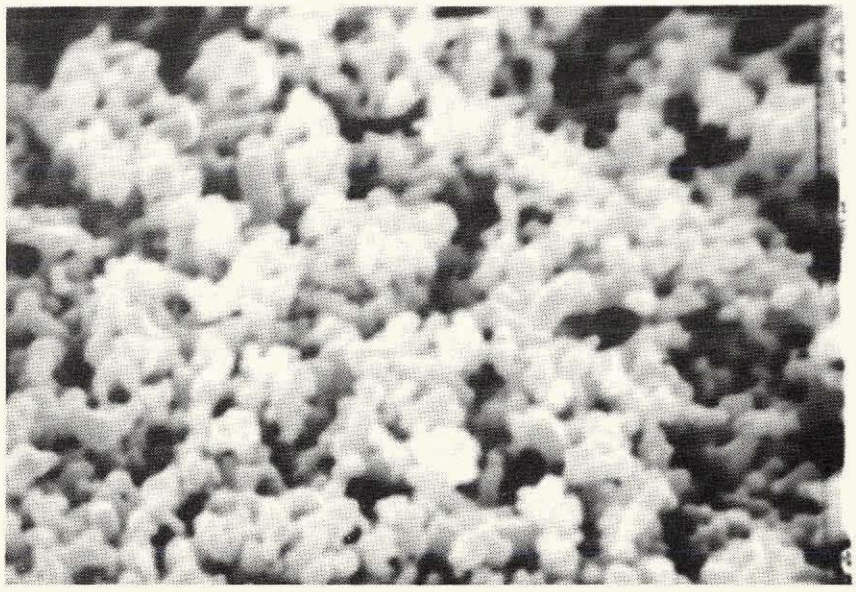

⟷ 0.5μ

Figure 21. Photograph of Specimen

CHAPTER III

RESULTS AND DISCUSSION

General

The limiting cases for reflection from rough surfaces are specular and diffuse. The ideal diffuse surface reflects according to Lambert's cosine law. For some rough materials the reflection can be divided into a specular and a diffuse component. This type of behavior is usually observed when the roughness is of the order of magnitude of the wavelength of radiation incident on the surface. In these instances the specular component can be obtained by subtracting the diffuse reflectance from reflectance measured in the specular direction.

The magnitude of the specular component is a strong function of incident angle and depending on the value of σ_o/λ it may be a function of wavelength. According to Fresnel's equations the specular reflectance will not be a function of wavelength when σ_o/λ is small enough so that the geometrical optics is applicable and the index of refraction is constant. In an absorbtion region for a nonconductor the absorbtion coefficient may not be zero according to Wendlandt, et.al. (16). Therefore, in an absorbtion region the additional requirement of constant absorbtion coefficient is needed to have the specular component independant of wavelength. For σ_o/λ

too large to use Fresnel's equations diffraction theory would be applicable. In this case the specular component for a perfect conductor can be shown to depend on wavelength, Davies (24). In general this would also be true for a nonconductor since diffraction is dependant upon σ_0/λ.

In general, the magnitude and distribution of the diffuse component depends on the roughness and wavelength. For rough nonconducting surfaces, especially powders, the diffuse reflectance depends greatly on the material optical properties, because in this case the particle size, index of refraction and absorbtance play a large role in controlling the diffuse reflectance.

The particle size of the ZnO used in this investigation was between 0.100 and 1.00 microns with mean size of 0.400 microns. This size distribution which was obtained from the National Aeronautics and Space Administration is verified by the scanning electron microscope photographs shown in Figures 20 and 21 of chapter II.

The photographs of the surface also show there are regions of different roughness scales, varying from about 10 microns to roughness the same order of magnitude as the particle size. According to Schatz (55) the transmission of a 0.76 micron layer of compacted ZnO is zero for wavelengths less than 0.500 microns and increases to about 30 percent for a wavelength of 1.70 micron. This and several other optical properties of ZnO are given in appendix B. Brown (51) gives a transmission of zero for wavelengths less than 0.500 microns

and 90 percent at 2.7 microns for a 0.9 micron layer of powder. This high transmission means the radiation can penetrate the surface facets as shown in Figure 22, and account for a very complex pattern of reflection. The particle size, roughness structure, and high transmission of particles would indicate an electromagnetic phenomena of reflection for this surface.

In the spectral region below 0.5 microns the index of refraction increases rapidly as wavelength decreases, going from 2.06 at 0.50 microns to 2.44 at 0.38 microns according to Bond (50) and Park (54).

Discussion of Reflectance

The reflectance results are shown in Figures 23 through 34 and are tabulated in Tables 5 through 28. The Tables also give the normalized reflectance divided by the cosine of the detector zenith, θ. The maximum detector zenith at which data could be taken was 85 degrees. When the detector azimuth was 180 degrees data could be taken within 7 degrees of the source zenith. Except for these limitations data could be taken in any direction. In order to obtain a good presentation of the diffuse component on the graph it was necessary to use two scales for axis of ordinates.

The diffuse component for all data above 0.400 microns correlate well with Lambert's law with the worst correlation occurring at a source zenith of 75 degrees. It is interesting that the diffuse component is essentially independent of wavelength for wavelengths

greater than 0.400 microns while the specular component changes with wavelength. This suggest the diffuse component is controlled by internal refraction and multiple scattering instead of just diffraction by ZnO particles; this agrees with the high particle transmission and the near constant index of refraction above 0.400 microns. The diffuse reflectance is characteristically different from the surface diffraction theory of Davies which could be, if internal phonemena is controlling the diffuse reflection. Also, this hypothesis is consistant with the phenomenal change in reflectance distribution between 0.350 and 0.400 microns. Since, in this region the index of refraction and absorbtion change considerably. This also implies geometrical optics would not be valid.

Figures 32 which is the variation of the reflectance at a detector zenith of zero degrees with source zenith shows there is little change in diffuse reflectance up to about 60 degrees. For source zeniths larger than 60 degrees apparently the specular reflection begins to drain much more energy causing a drop in the diffuse component for wavelengths above 0.400 microns. However, the curve for data at 0.300 microns is concave upward which is completely different from the data above 0.400 microns.

Figure 27 which is the variation of bidirectional reflectance with source azimuth shows the reflectance is essentially independent of source azimuth. Also, Table 12 shows the surface does not reflect in any preferred direction.

The variation in diffuse reflectance with wavelength is given in Figure 34. This distribution is in agreement with other investigations for the hemispherical reflectance. According to Gilligan (51) the absorption process below 0.400 microns is that of raising a valence band electron to a conduction band. The column D_s/D_p under the heading ZnO in Table 27 shows the reflectance for a source incident angle of 30 degrees is independent of polarization above 0.400 microns. As will be discussed below the reflectance as a function of detector zenith depends on polarization. Below 0.400 microns the surface selectively absorbs the polarized components. While this does not completely account for the reflectance distribution it does appear to be an integral part of the reflection phenomena.

As shown in Figures 29 and 30, the variation of the diffuse component with polarization is significant at all wavelengths. This along with the variation of the specular component with polarization is further evidence that electromagnetic theory is applicable.

Figure 33 which is the specular component shows this component is not simply due to reflection from the smooth sides of the ZnO crystals. Since in this case for ZnO the index of refraction is constant and Fresnel's equations predict a specular reflection independent of wavelength which is contradictory to the specular data.

Another characteristic of the data is backscatter in the vicinity of the source zenith. Experimental evidence of this phenomenon

have been observed by other investigators. The backscatter is the reflectance in the vicinity of the source direction minus the diffuse reflection in the same direction. The data obtained for P-Plane polarized source and the data at 0.300 micron exhibit the most back-scatter as shown in figure 30.

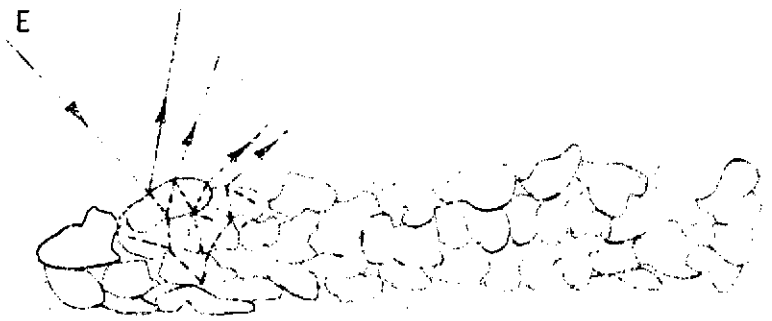

Figure 22. Reflection from Powder

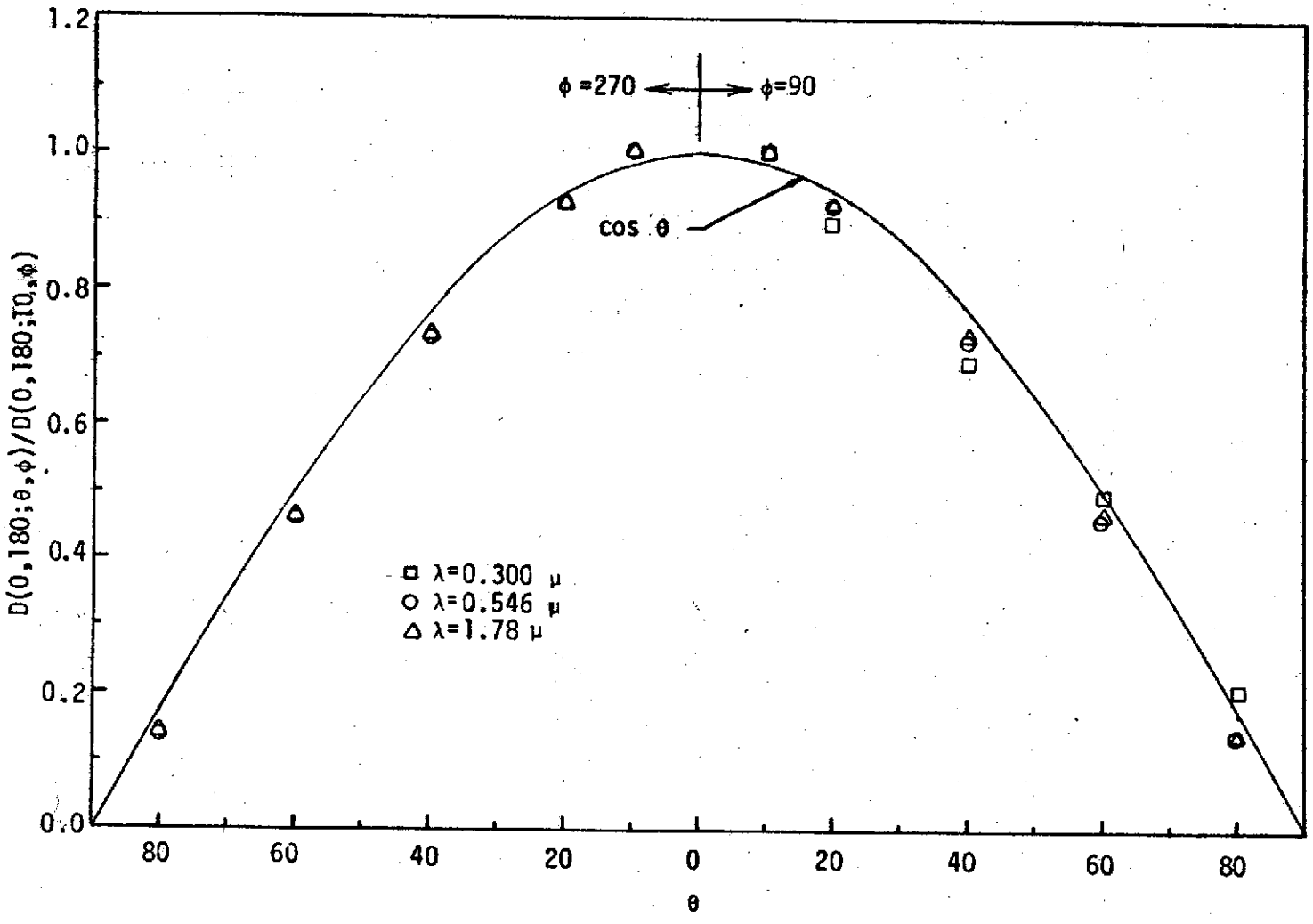

Figure 23. Reflectance of ZnO

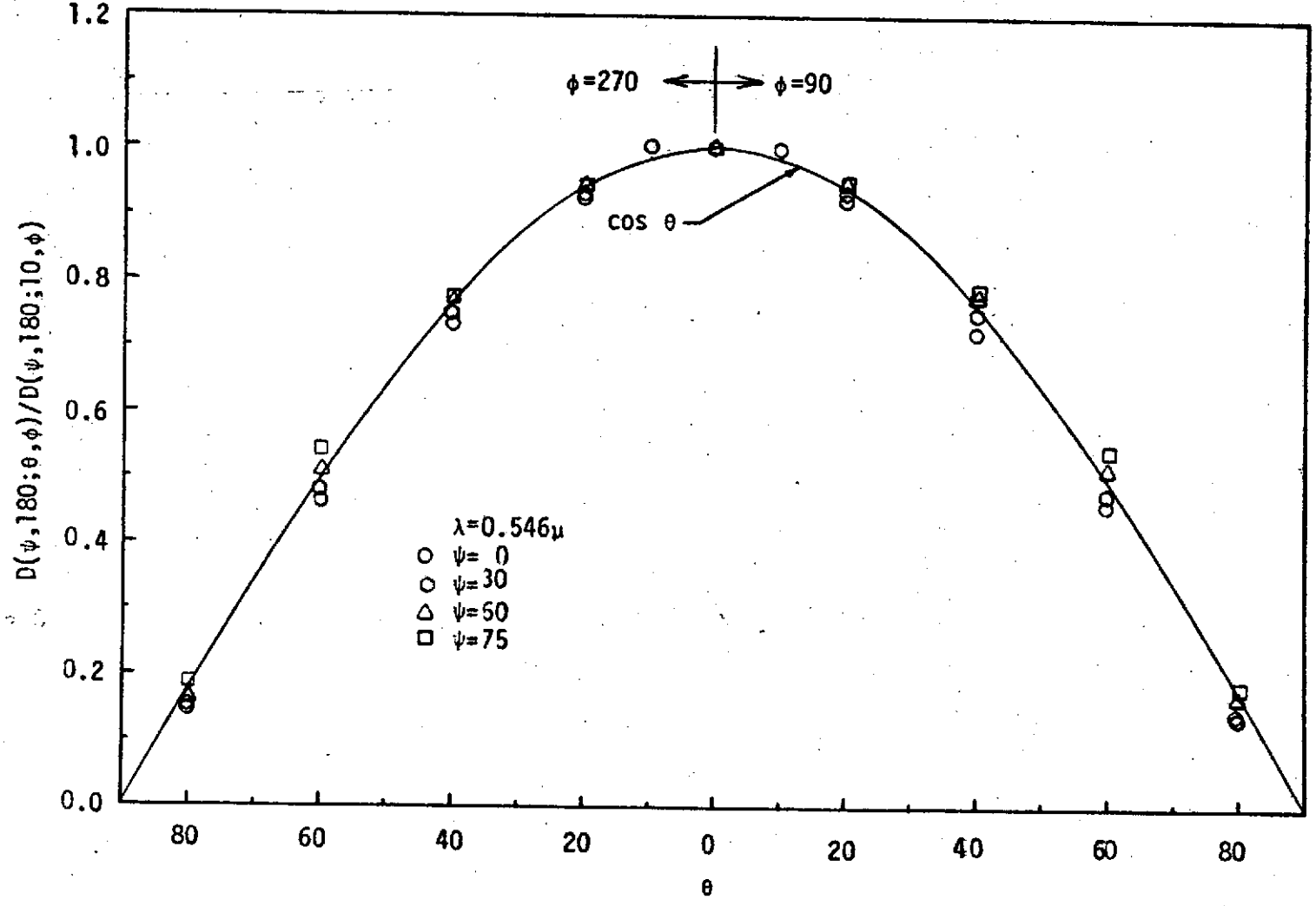

Figure 24. Reflectance of ZnO

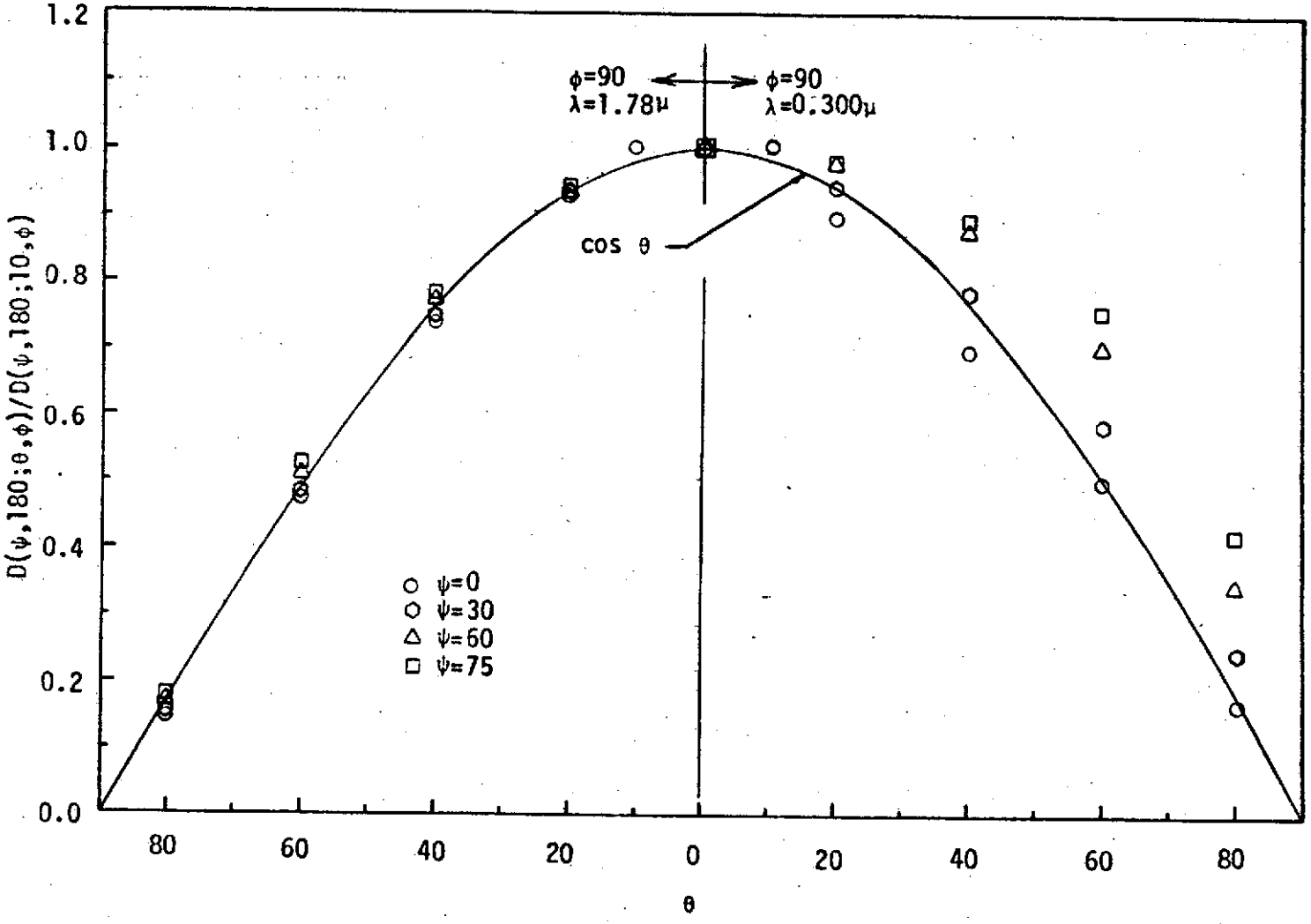

Figure 25. Reflectance of ZnO

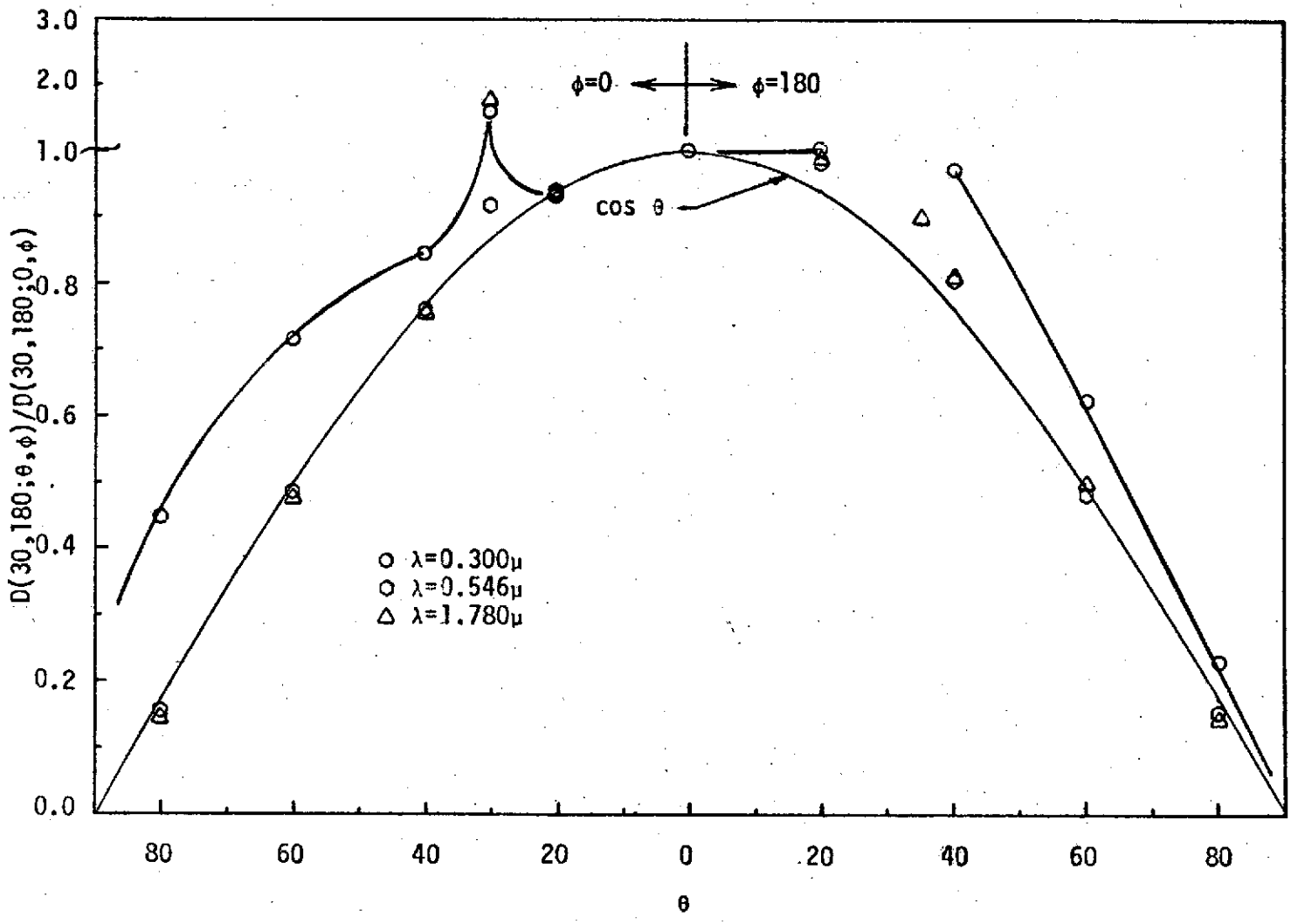

Figure 26. Reflectance of ZnO

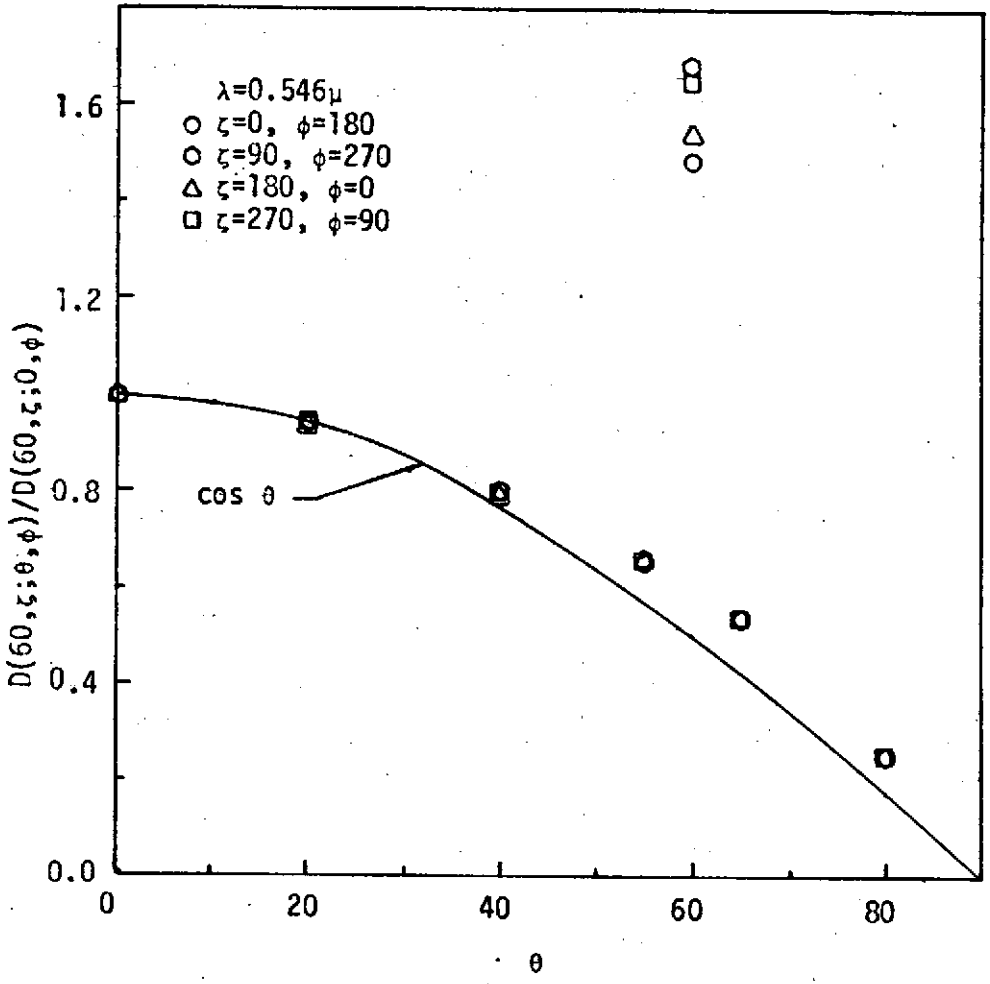

Figure 27. Reflectance of ZnO

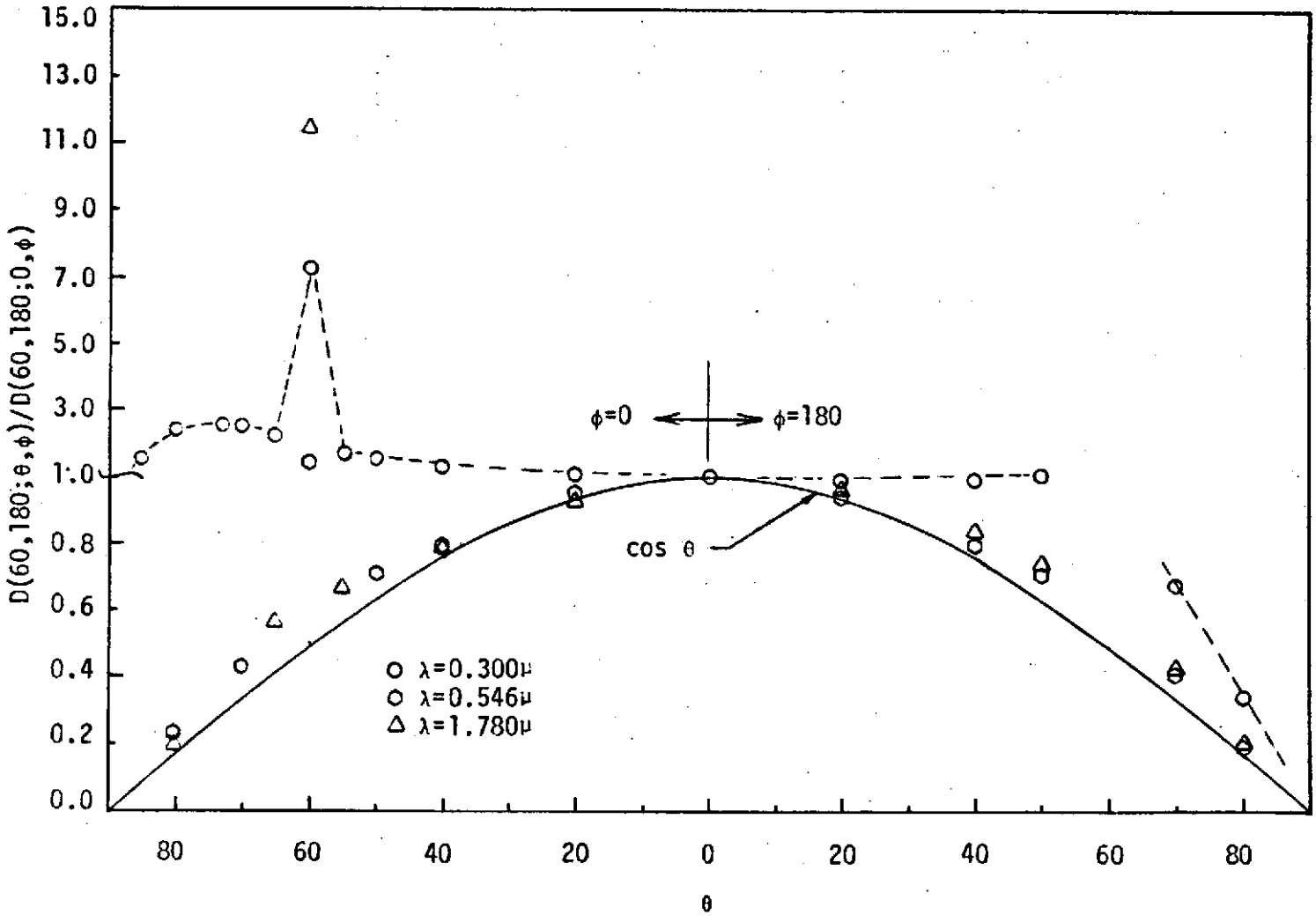

Figure 28. Reflectance of ZnO

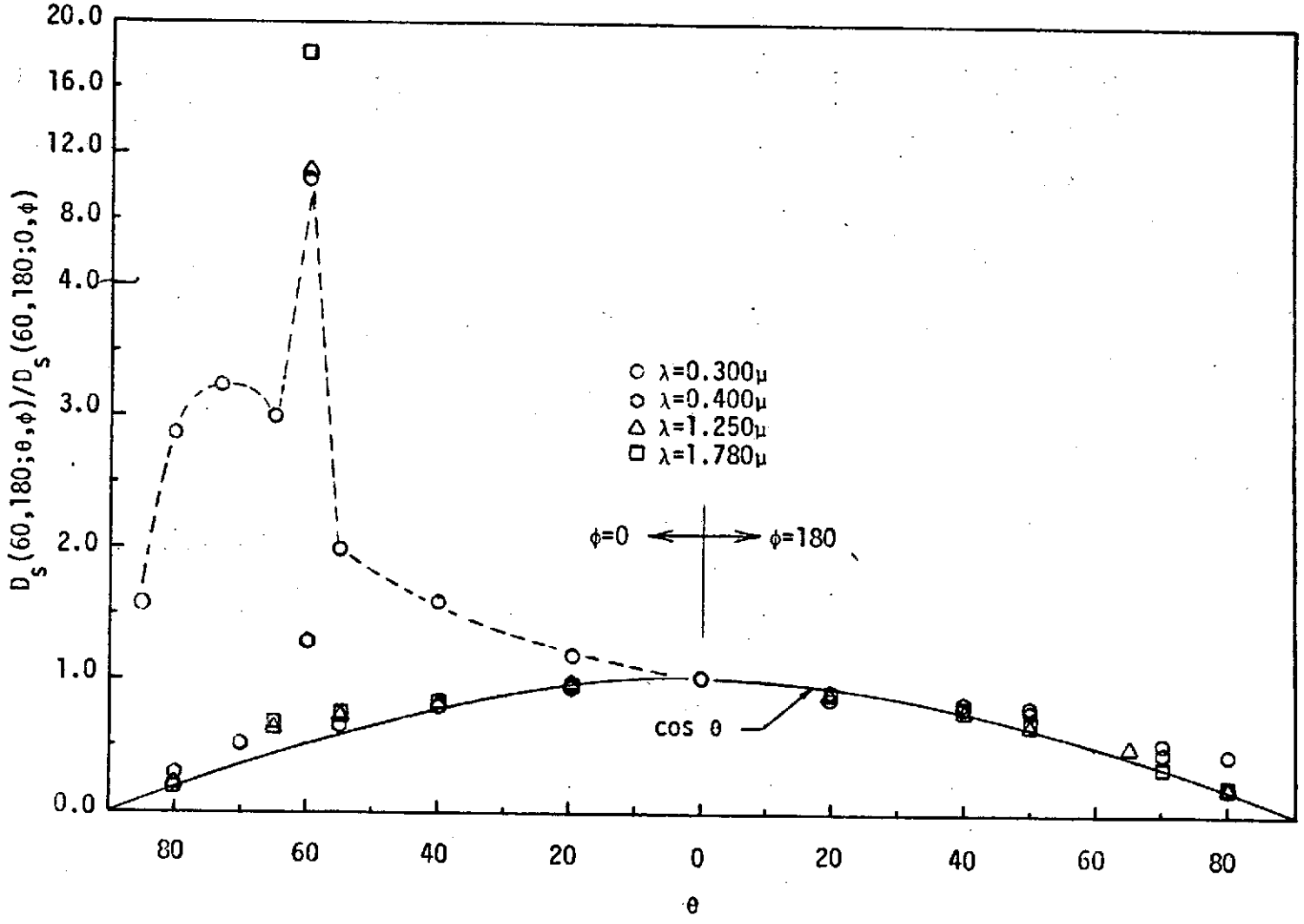

Figure 29. Reflectance of ZnO for Source Polarized in S-Plane

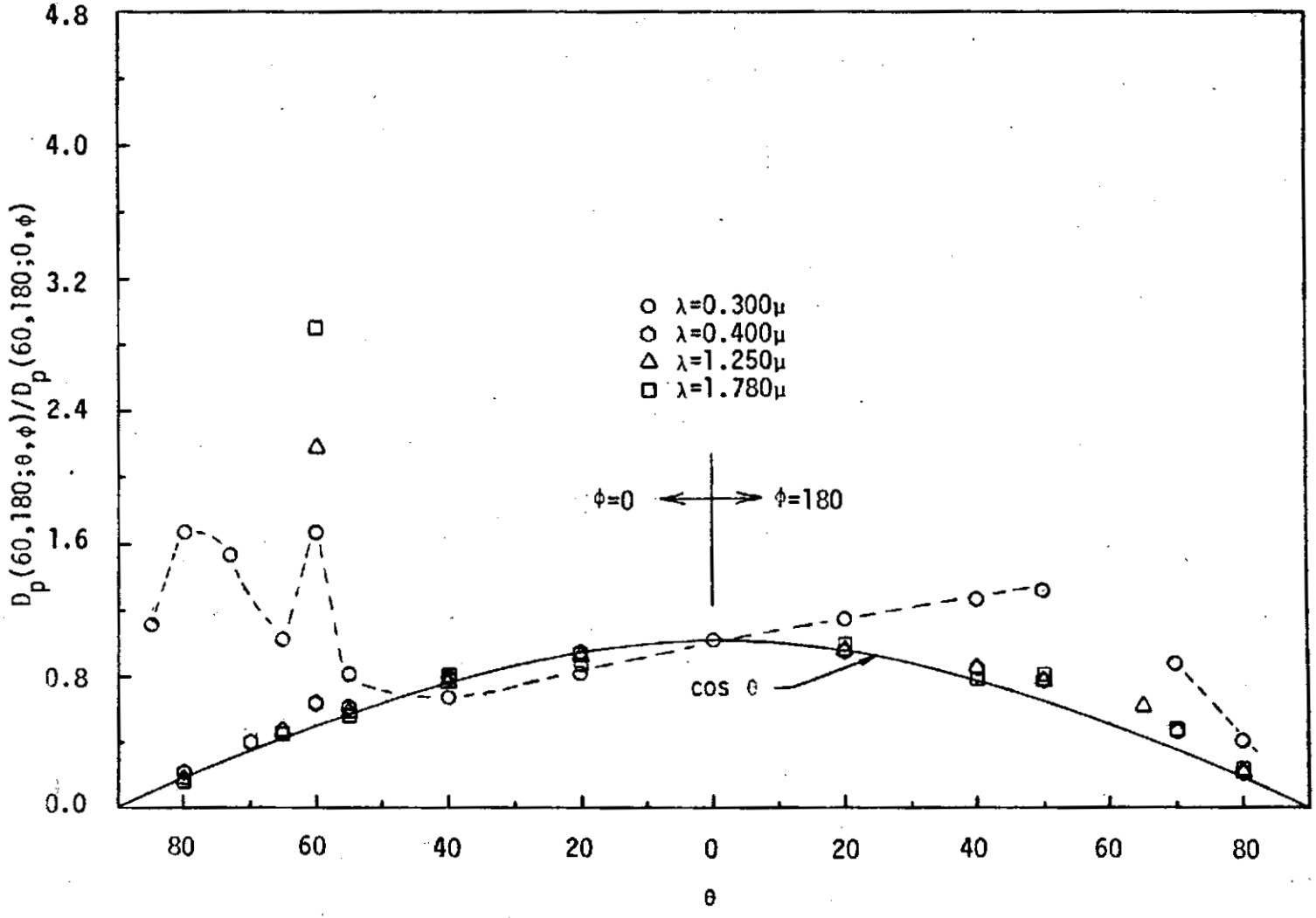

Figure 30. Reflectance of ZnO for Source Polarized in P-Plane

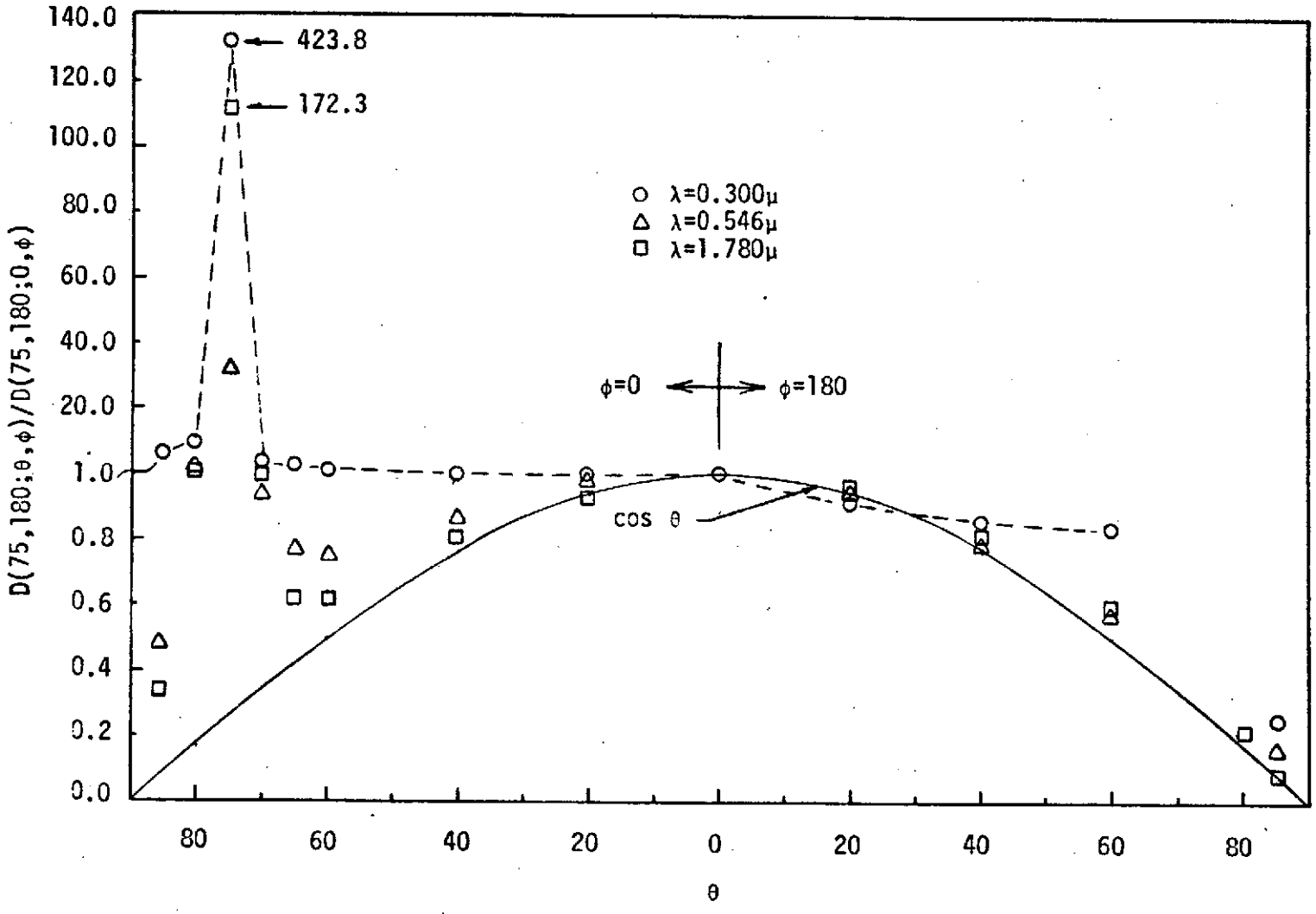

Figure 31. Reflectance of ZnO

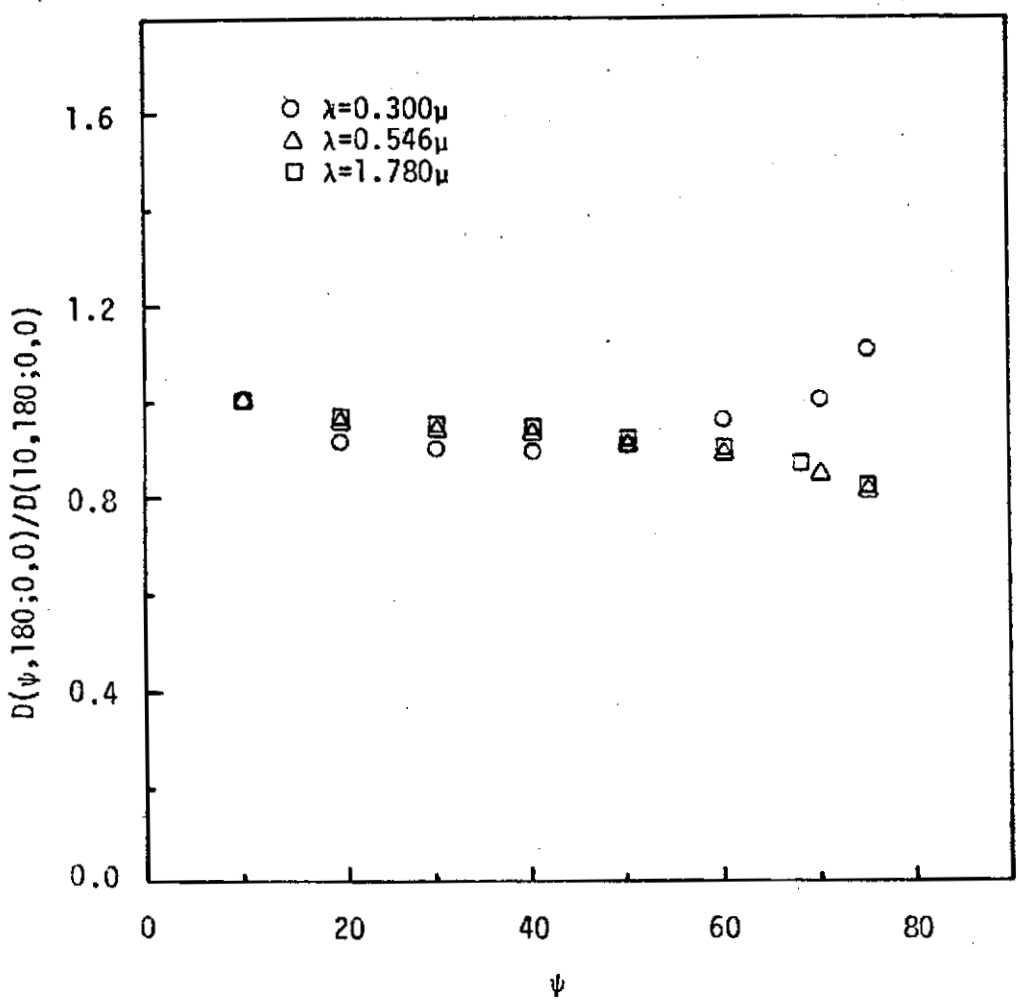

Figure 32. Reflectance of ZnO Versus Source Incidence Angle

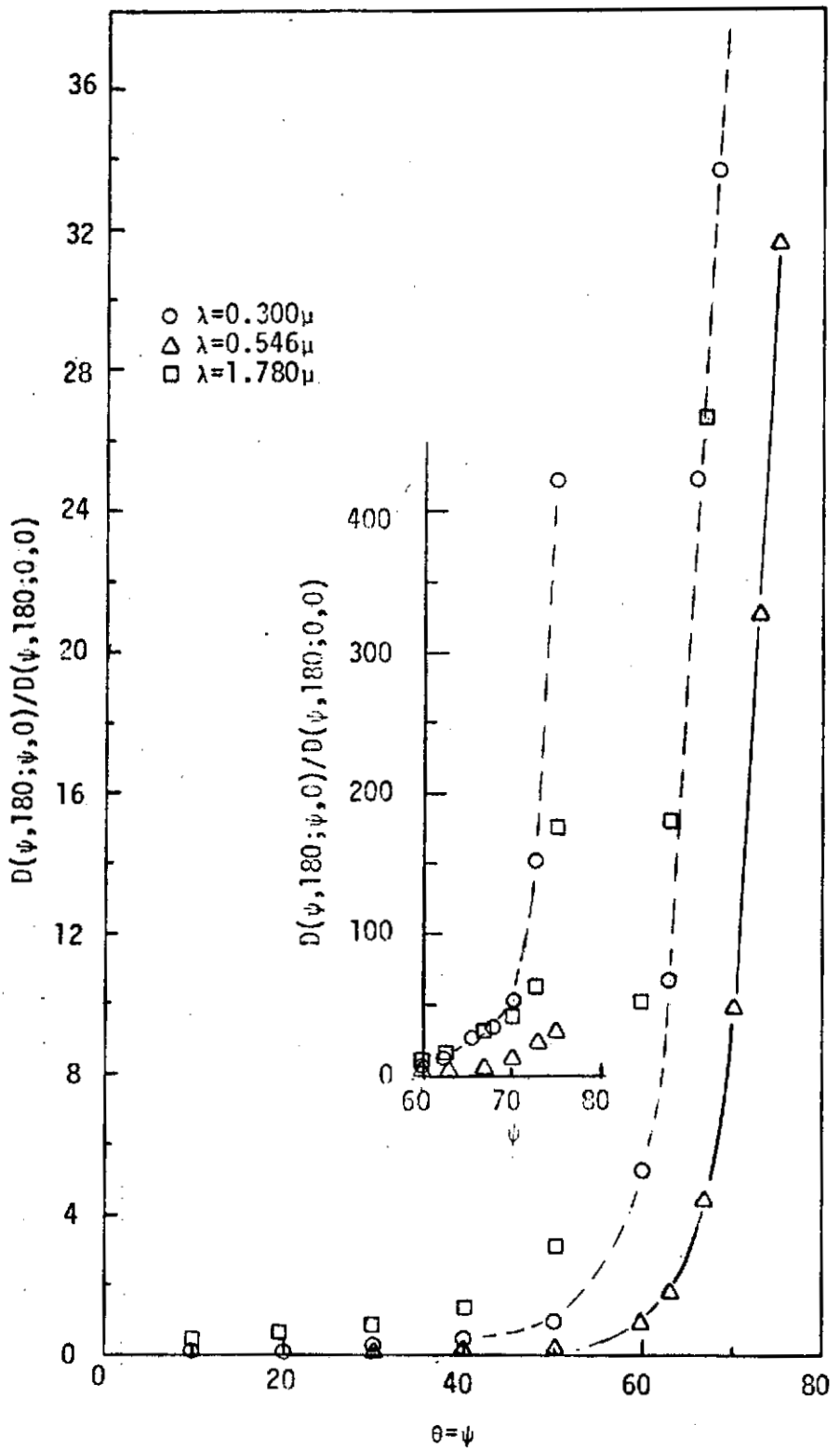

Figure 33. Specular Reflectance

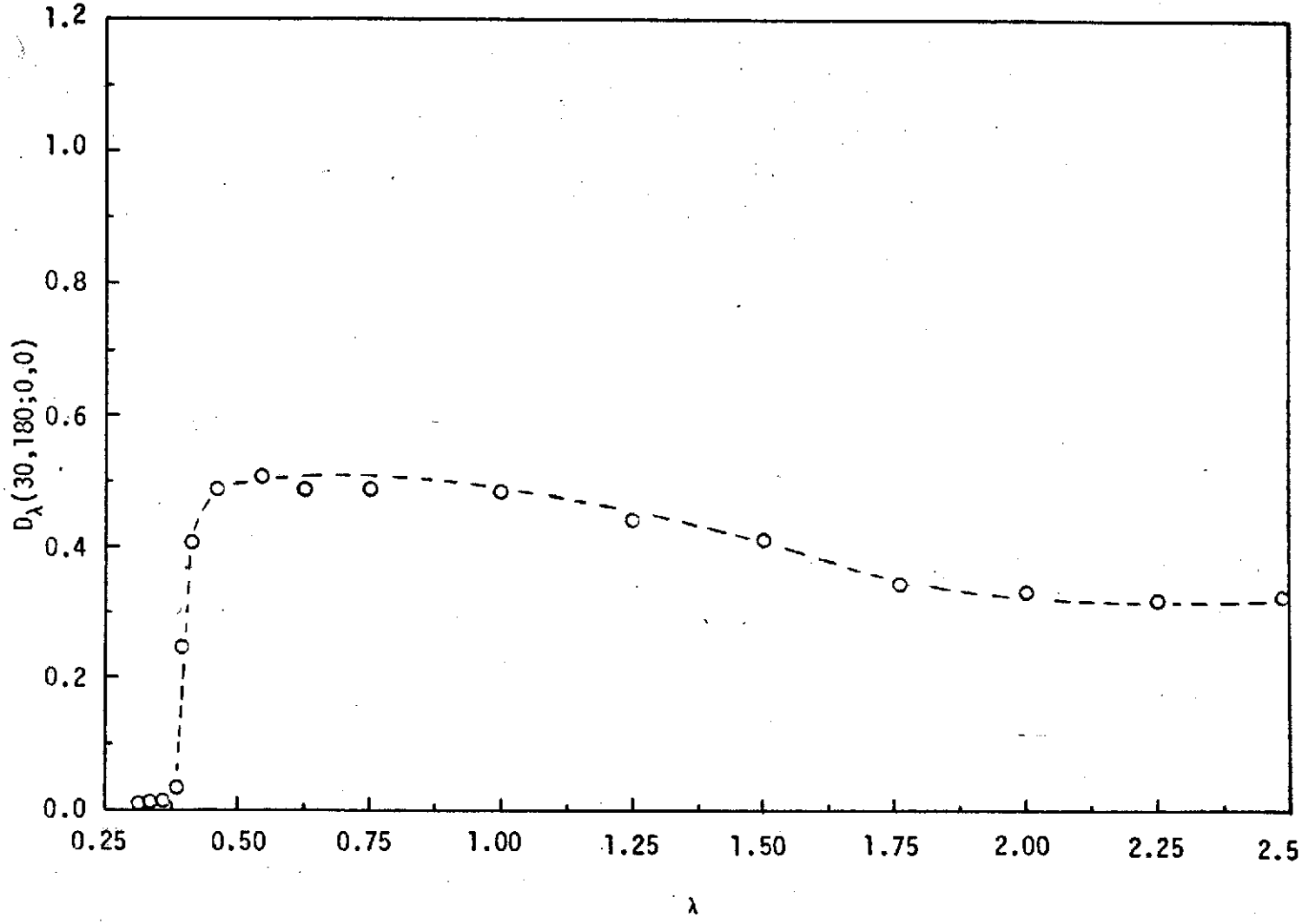

Figure 34. Variation of Reflectance with Wavelength

TABLE 5

REFLECTANCE OF ZnO AT 0.300 MICRONS

$D(0°,180°;\theta,\phi)/D(0°,180°;10°,\phi)$

θ	$\phi=0°$	$\phi=90°$	$\phi=180°$
10	1.000*	1.000	1.000
	1.015	1.015	1.015
20	0.891	0.894	0.889
	0.951	0.951	0.946
40	0.696	0.696	0.695
	0.909	0.910	0.907
60	0.501	0.495	0.501
	1.002	0.990	1.002
80	0.217	0.212	0.217
	1.247	1.218	1.247

*Upper value is ρ_n and lower value is ρ as defined on page 2.

TABLE 5

REFLECTANCE OF ZnO AT 0.300 MICRONS

$D(30^\circ,180^\circ;\theta,\phi)/D(30^\circ,180^\circ;0^\circ,\phi)$

θ	$\phi=0^\circ$	$\phi=90^\circ$	$\phi=180^\circ$
0	1.000	1.000	1.000
20	0.930 0.989	0.942 1.002	1.057 1.124
30	1.520 1.755	-	-
40	0.848 1.107	0.788 1.029	0.978 1.277
60	0.716 1.432	0.583 1.166	0.624 1.248
80	0.449 2.500	0.240 1.379	0.232 1.333

TABLE 7

REFLECTANCE OF ZnO AT 0.300 MICRONS

$D(60^\circ,180^\circ;\theta,\phi)/D(60^\circ,180^\circ;0^\circ,\phi)$

θ	$\phi=0^\circ$	$\phi=90^\circ$	$\phi=180^\circ$
0	1.000	1.000	1.000
20	1.071 1.139	0.975 1.037	0.986 1.049
40	1.276 1.666	0.877 1.145	0.988 1.290
50	1.512 2.351	-	0.998 1.552
55	1.684 2.934	-	-
60	7.239 14.418	0.699 1.398	-
65	2.239 5.293	-	-
70	2.485 7.266	-	0.677 1.980
73	2.475 8.476	-	-
80	2.441 14.029	0.330 1.897	0.340 1.954
85	1.455 16.724	-	

TABLE 8

REFLECTANCE OF ZnO WITH SOURCE POLARIZED
IN S AND P PLANES AT 0.300 MICRONS

$D(60^\circ, 180^\circ; \theta, \phi)/D(60^\circ, 180^\circ; 0^\circ, \phi)$

	S-Plane		P-Plane	
θ	$\phi=0^\circ$	$\phi=180^\circ$	$\phi=0^\circ$	$\phi=180^\circ$
0	1.000	1.000	1.000	1.000
20	1.216 1.294	0.875 0.931	0.814 0.866	1.155 1.229
40	1.608 2.099	0.821 1.072	0.682 0.890	1.261 1.646
50	-	0.816 1.269	-	1.303 2.026
55	2.032 3.540	-	0.801 1.395	-
60	10.531 21.062	-	1.670 3.340	-
65	2.981 7.470	-	1.075 2.541	-
70	-	0.556 1.626	-	0.864 2.526
73	3.258 11.156	-	1.522 5.212	-
80	2.874 16.517	0.281 1.615	1.656 9.517	0.443 2.546
85	1.573 18.080	-	1.130 13.092	-

TABLE 9

REFLECTANCE OF ZnO AT 0.300 MICRONS

$D(75°,180°;\theta,\phi)/D(75°,180°;0°,\phi)$

θ	$\phi=0°$	$\phi=90°$	$\phi=180°$
0	1.000	1.000	1.000
20	1.104 1.174	0.975 1.037	0.913 0.971
40	1.085 1.416	0.895 1.168	0.854 1.115
60	1.879 3.758	0.753 1.506	0.839 1.678
65	2.656 6.279	-	0.834 1.972
70	4.429 12.950	-	-
75	423.800 1631.000	-	-
80	8.129 46.718	0.413 2.374	-
85	5.211 59.897	-	0.257 2.954

TABLE 10

REFLECTANCE OF ZnO WITH SOURCE POLARIZED
IN S AND P PLANE AT 0.350 MICRONS

$D(60°,180°;\theta,\phi)/D(60°,180°;0,\phi)$

	S-Plane		P-Plane	
θ	φ=0°	φ=180°	φ=0°	φ=180°
0	1.000	1.000	1.000	1.000
20	1.216 1.294	0.877 0.933	0.819 0.871	1.151 1.224
40	1.588 2.073	0.816 1.065	0.672 0.877	1.246 1.627
50	-	0.807 1.255	-	1.274 1.981
55	2.269 3.953	-	0.757 1.319	-
60	10.889 21.778	-	1.970 3.940	-
65	2.995 7.080	-	1.059 2.504	-
70	-	0.648 1.895	-	0.867 2.541
73	3.130 10.719	-	1.386 4.747	-
80	2.720 15.632	0 .272 15.632	1.642 9.437	0.430 2.471
85	2.020 23.218	-	.997 11.460	-

TABLE 11

REFLECTANCE OF ZnO WITH SOURCE POLARIZED
IN S AND P PLANES AT 0.400 MICRONS

$D(60^\circ,180^\circ;\theta,\phi)/D(60^\circ,180^\circ;0^\circ,\phi)$

	S-Plane		P-Plane	
θ	$\phi=0^\circ$	$\phi=180^\circ$	$\phi=0^\circ$	$\phi=180^\circ$
0	1.000	1.000	1.000	1.000
20	0.953 1.014	0.961 1.022	0.937 0.997	0.967 1.029
40	0.821 1.072	0.845 1.103	0.775 1.012	0.844 1.102
50	-	0.794 1.235	-	0.789 1.227
55	0.687 1.197	-	0.606 1.056	-
60	1.314 2.627	-	0.636 1.272	-
70	.514 1.503	0.461 1.348	0.406 1.187	0.459 1.342
80	.303 1.741	0.209 1.201	0.228 1.310	0.209 1.201

TABLE 12

REFLECTANCE OF ZnO AT 0.546 MICRONS

$D(0^\circ,180^\circ;\theta,\phi)/D(0^\circ,180;10,\phi)$

θ	$\phi=0^\circ$	$\phi=90^\circ$	$\phi=180^\circ$	$\phi=270^\circ$
10	1.000	1.000	1.000	1.000
20	0.923	0.920	0.929	0.921
	0.982	0.979	0.988	0.980
40	0.728	0.720	0.730	0.727
	0.950	0.940	0.953	0.949
60	0.470	0.458	0.455	0.460
	0.940	0.916	0.910	0.920
80	0.140	0.137	0.142	0.142
	0.805	0.787	0.816	0.816

TABLE 13

REFLECTANCE OF ZnO AT 0.546 MICRONS

$D(30^\circ,180^\circ;\theta,\phi)/D(30^\circ,180^\circ;0,\phi)$

θ	$\phi=0^\circ$	$\phi=90^\circ$	$\phi=180^\circ$	$\phi=270^\circ$
0	1.000	1.000	1.000	1.000
20	0.942 1.002	0.938 0.998	0.981 1.044	0.932 0.991
30	0.918 1.060	-	-	-
40	0.762 0.995	0.751 0.980	0.808 1.055	0.751 0.980
60	0.489 0.978	0.481 0.962	0.487 0.974	0.482 0.964
80	0.155 0.891	0.148 0.851	0.156 0.897	0.151 0.868

TABLE 14

VARIATION OF REFLECTANCE WITH SOURCE AZIMUTH AT 0.546 MICRONS

$D(60^\circ,\zeta;\theta,\phi)/D(60^\circ,\zeta;0^\circ,\phi)$

θ	$\phi=180^\circ$ $\zeta=0^\circ$	$\phi=270^\circ$ $\zeta=90^\circ$	$\phi=0^\circ$ $\zeta=180^\circ$	$\phi=90^\circ$ $\zeta=270^\circ$
0	1.000	1.000	1.000	1.000
20	0.954 1.015	0.950 1.011	0.943 1.003	0.954 1.015
40	0.805 1.051	0.803 1.048	0.793 1.035	0.803 1.048
55	0.655 1.141	0.654 1.139	0.657 1.145	0.654 1.139
60	1.490 2.980	1.690 3.380	1.540 3.080	1.650 3.300
65	0.539 1.274	0.537 1.270	0.537 1.270	0.540 1.277
80	0.251 1.443	0.250 1.437	0.249 1.431	0.245 1.408

TABLE 15

REFLECTION OF ZnO AT 0.546 MICRONS

$D(60^\circ,180^\circ;\theta,\phi)/D(60,180;0^\circ,\phi)$

θ	$\phi=0$	$\phi=0^\circ$	$\phi=180^\circ$	$\phi=180^\circ$
0	1.000	1.000	1.000	1.000
20	0.955 1.016	0.957 1.018	0.946 1.006	0.941 1.001
40	0.790 1.031	0.801 1.046	0.793 1.035	0.791 1.033
50	0.701 1.090	0.708 1.101	0.715 1.112	0.711 1.309
55	-	0.661 1.152	-	-
60	1.490 2.980	1.540 3.080	-	-
65	-	0.544 1.286	-	-
70	0.435 1.272	-	0.400 1.170	0.407 1.190
80	0.240 1.379	0.250 1.437	0.181 1.040	0.185 1.063

TABLE 16

REFLECTANCE OF ZnO AT 0.546 MICRONS

$D(60^\circ,180^\circ;\theta,\phi)/D(60^\circ,180^\circ;0^\circ,\phi)$

θ	$\phi=90^\circ$	$\phi=270^\circ$
0	1.000	1.000
20	0.943 1.003	0.942 1.002
40	0.774 1.010	0.771 1.007
60	0.518 1.036	0.514 1.028
80	0.170 0.997	0.167 0.970

TABLE 17

REFLECTANCE OF ZnO WITH SOURCE POLARIZED
IN S AND P PLANES AT 0.546 MICRONS

$D(60^\circ,180^\circ;\theta,\phi)/D(60^\circ,180^\circ;0^\circ,\phi)$

	S-Plane		P-Plane	
θ	$\phi=0^\circ$	$\phi=180^\circ$	$\phi=0^\circ$	$\phi=180^\circ$
0	1.000	1.000	1.000	1.000
20	0.960 1.021	0.939 0.999	0.952 1.013	0.952 1.013
40	0.815 1.064	0.787 1.027	0.790 1.031	0.801 1.046
50	0.725 1.128	0.656 1.020	0.693 1.078	0.721 1.121
60	2.130 4.260	-	0.853 1.706	-
70	0.509 1.488	0.408 1.193	0.406 1.187	0.403 1.178
80	0.274 1.575	0.177 1.017	.221 1.270	0.182 1.046

TABLE 18

REFLECTANCE OF ZnO AT 0.546 MICRONS

$D(75^\circ,180^\circ;\theta,\phi)/D(75^\circ,180^\circ;0^\circ,\phi)$

θ	$\phi=0^\circ$	$\phi=90^\circ$	$\phi=180^\circ$	$\phi=270^\circ$
0	1.000	1.000	1.000	1.000
20	0.971 1.033	0.949 1.064	0.928 0.987	0.948 1.009
40	0.863 1.127	0.786 1.026	0.781 1.020	0.790 1.031
60	0.749 1.496	0.546 1.080	0.572 1.144	0.541 1.082
65	0.769 1.818	-	0.532 1.258	-
70	0.945 2.763	-	-	-
75	31.680 122.100	-	-	-
80	1.520 8.736	0.189 1.086	-	0.196 1.126
85	0.471 5.414	-	0.165 1.897	-

TABLE 19

REFLECTANCE OF ZnO WITH SOURCE POLARIZED
IN S AND P PLANES AT 1.25 MICRONS

$D(60^\circ,180^\circ;\theta,\phi)/D(60^\circ,180^\circ;0^\circ,\phi)$

	S-Plane		P-Plane	
θ	$\phi=0^\circ$	$\phi=180^\circ$	$\phi=0^\circ$	$\phi=180^\circ$
0	1.000	1.000	1.000	1.000
20	0.973 1.035	0.904 0.962	0.922 0.981	0.983 1.046
40	0.847 1.106	0.762 0.995	0.746 0.974	0.853 1.114
50	-	0.679 1.056	-	0.770 1.198
55	0.746 1.300	-	0.583 1.016	-
60	10.950 21.900	-	2.179 4.358	-
65	0.641 1.515	0.523 1.236	0.470 1.111	0.618 1.461
80	0.237 1.362	0.176 1.011	0.195 1.121	0.201 1.155

TABLE 20

REFLECTANCE OF ZnO AT 1.78 MICRONS

$D(0^\circ,180;\theta,\phi)/D(0^\circ,180^\circ;10^\circ,\phi)$

θ	$\phi=0^\circ$	$\phi=90^\circ$	$\phi=180^\circ$	$\phi=270^\circ$
10	1.000	1.000	1.000	1.000
20	0.924	0.928	0.922	0.925
	0.983	0.987	0.981	0.984
40	0.732	0.734	0.735	0.737
	0.956	0.958	0.960	0.962
60	0.468	0.471	0.467	0.465
	0.936	0.942	0.934	0.930
80	0.139	0.145	0.142	0.146
	0.799	0.833	0.816	0.839

TABLE 21

REFLECTANCE OF ZnO AT 1.78 MICRONS

$D(30^\circ,180^\circ;\theta,\phi)/D(30^\circ,180^\circ;0^\circ,\phi)$

θ	$\phi=0^\circ$	$\phi=90^\circ$	$\phi=180^\circ$
0	1.000	1.000	1.000
20	0.919 0.978	0.931 0.990	0.987 1.050
30	1.770 2.044	-	-
35	-	-	0.904 1.104
40	0.752 0.982	0.747 0.975	0.812 1.060
60	0.474 0.948	0.482 0.964	0.506 1.012
80	0.145 0.833	0.154 0.885	0.149 0.856

TABLE 22

REFLECTANCE OF ZnO AT 1.78 MICRONS

$D(60^{\circ},180^{\circ};\theta,\phi)/D(60^{\circ},180^{\circ};0^{\circ},\phi)$

θ	$\phi=0^{\circ}$	$\phi=90^{\circ}$	$\phi=180^{\circ}$
0	1.000	1.000	1.000
20	0.933 0.993	0.935 0.995	0.967 1.029
40	0.783 1.022	0.773 1.009	0.839 1.095
50	-	-	0.742 1.154
55	0.664 1.157	-	-
60	11.410 22.820	0.510 1.020	-
65	0.566 1.338	-	-
70	-	-	0.424 1.240
80	0.200 1.149	0.170 0.977	0.206 1.184

TABLE 23

REFLECTANCE OF ZnO WITH SOURCE POLARIZED IN S AND P-PLANES AT 1.78 MICRONS

$D(60^\circ,180^\circ;\theta,\phi)/D(60^\circ,180^\circ;0^\circ,\phi)$

	S-Plane		P-Plane	
θ	$\phi=0^\circ$	$\phi=180^\circ$	$\phi=0^\circ$	$\phi=180^\circ$
0	1.000	1.000	1.000	1.000
20	0.968 1.030	0.933 0.993	0.897 0.954	1.005 1.069
40	0.847 1.106	0.786 1.026	0.743 0.956	0.783 1.166
50	-	0.686 1.067	-	0.803 1.249
55	0.764 1.331	-	0.573 0.998	-
60	18.250 36.500	-	2.940 5.880	-
65	0.679 1.605	-	0.461 1.090	-
70	-	0.387 1.132	-	0.470 1.374
80	0.224 1.287	0.189 1.086	0.178 1.023	0.226 1.299

TABLE 24

REFLECTANCE OF ZnO AT 1.78 MICRONS

$D(75^\circ,180^\circ;\theta,\phi)/D(75^\circ,180^\circ;0^\circ,\phi)$

θ	$\phi=0^\circ$	$\phi=90^\circ$	$\phi=180^\circ$
0	1.000	1.000	1.000
20	0.938 0.998	0.939 0.999	0.961 1.022
40	0.806 1.052	0.784 1.023	0.825 1.077
60	0.616 1.232	0.525 1.050	0.594 1.188
65	0.625 1.478	-	-
70	0.999 2.912	-	0.528 1.544
75	172.300 666.000	-	-
80	1.150 66.090	0.177 1.017	0.226 1.299
85	0.330 3.793	-	0.085 0.977

TABLE 25

REFLECTANCE OF ZnO WITH SOURCE POLARIZED IN S AND P-PLANES AT 2.5 MICRONS

$D(60^\circ, 180^\circ; \theta, \phi)/D(60^\circ, 180^\circ; 0^\circ, \phi)$

	S-Plane		P-Plane	
θ	$\phi=0^\circ$	$\phi=180^\circ$	$\phi=0^\circ$	$\phi=180^\circ$
0	1.000	1.000	1.000	1.000
20	0.934 0.994	0.942 1.002	0.921 0.980	0.989 1.052
40	0.811 1.059	0.794 1.037	0.793 1.035	0.855 1.305
50	-	0.703 1.093	-	0.763 1.187
55	0.793 1.382	-	0.670 1.167	-
60	30.370 6.074	-	0.748 1.496	-
65	0.716 1.693	0.472 1.116	0.587 1.388	0.528 1.248
80	0.200 1.149	0.166 0.954	0.156 .897	0.203 1.167

TABLE 26

VARIATION OF REFLECTANCE WITH SOURCE INCIDENT ANGLE

$D(\psi, 180^\circ; 0^\circ, 0^\circ)/D(10^\circ, 180^\circ; 0^\circ, 0)$

Incidence Angle	Wavelength-microns 0.300	0.540	1.780
10	1.000	1.000	1.000
20	0.920	0.960	0.966
30	0.895	0.942	0.953
40	0.890	0.928	0.939
50	0.912	0.910	0.923
60	0.965	0.887	0.899
68	-	-	0.872
70	1.056	0.848	-
75	1.107	0.810	0 .817

TABLE 27

SPECULAR REFLECTANCE
$D(\psi,180°;\psi,0°)/D(\psi,180°;0°,0°)$

	Wavelength-microns		
θ	0.300	0.546	1.780
10	0.132	0.0	0.553
20	0.140	0.0	0.647
30	0.270	0.080	0.852
40	0.329	0.106	1.370
50	0.910	0.222	3.141
60	5.238	0.968	10.040
63	10.750	1.819	15.120
66	24.900	-	-
67	-	4.450	26.609
68	33.600	-	-
70	53.110	9.872	40.858
73	151.240	21.157	64.827
75	423.800	31.680	172.300

TABLE 28

VARIATION OF REFLECTANCE WITH WAVELENGTH*

	Source	ZnO		
λ	D_p/D_s	D_p/D_s	$D_{p,ZnO}/D_{p,source}$	D_λ
0.300	0.985	0.609	0.010	0.013
0.325	1.090	0.578	0.010	0.014
0.350	1.110	0.608	0.011	0.015
0.375	0.964	0.934	0.074	0.077
0.385	0.886	1.018	0.250	0.240
0.400	0.862	1.009	0.407	0.405
0.450	0.767	1.046	0.495	0.484
0.546	0.638	0.987	0.506	0.509
0.625	0.679	1.018	0.488	0.484
0.750	0.571	1.009	0.491	0.489
1.000	0.400	0.995	0.480	0.481
1.250	1.720	0.998	0.440	0.443
1.500	2.830	0.975	0.406	0.411
1.780	1.041	0.998	0.345	0.345
2.000	0.887	0.989	0.333	0.335
2.250	0.790	0.991	0.319	0.321
2.500	2.740	0.960	0.319	0.326

*$\psi = 30°$, $\zeta = 180°$, $\theta = 0°$, $\phi = 0°$

CHAPTER IV

CONCLUSIONS AND RECOMENDATIONS

The results of this investigation can be summarized as follows:

1. σ_o/λ varies over the surface with $\sigma_o/\lambda \sim 1$ in some regions and $\sigma_o/\lambda > 1$ in other regions. Therefore we cannot speak of a single roughness which characterize the entire surface and it is necessary to specifically define a local roughness.
2. Because of the order of magnitude of σ_o/λ, Electromagnetic Theory is suggested to explain the reflection phenomena. This is confirmed by the variation of the specular component with wavelength and the variation of reflectance with polarization.
3. Figure 21 indicates that the high transmission of the ZnO particles which is given in Table B-1 causes a multiple refraction and this indicates that the diffuse reflection is largely controlled by internal phenomena of the material. As a result there is a substantial change in reflectance with wavelength near 0.400 microns where the index of refraction and reflectance change rapidly with wavelength.
4. The multiple refraction of ZnO particles can explain the phenomena of backscatter.

5. The diffuse reflectance above 0.400 microns is close to a Lambert surface.

The phenomena of reflection from powder specimens is so complex that for engineering purposes it is most fruitful to investigate the bidirectional reflectance by experimental means. However, the available results from theory was used to explain trends in behavior in the reflectance data.

The purpose of this investigation was to determine original and accurate bidirectional reflectance data of ZnO. Since ZnO is used as a paint pigment one possible application of these results would be to further the understanding of reflectance phenomena in which it is a pigment. A possible logical extention of this work is to investigate bidirectional reflectance data of such paints and compare with the results of this investigation.

To further understand the reflection phenomena of ZnO it is recommended that research be conducted with ZnO of different particle shape and size. Also, to determine what role, if any, the size plays in the change in reflectance characteristic near 0.400 microns.

APPENDIX A

ERROR ANALYSIS

The purpose of this error analysis is to determine the validity and accuracy of the test data. The analysis is divided into three parts; general validity, repeatability and uncertainty analysis.

In order to determine the general validity of the experimental apparatus data was taken using a smoked magnesium oxide specimen. This data were compared to that of Brandenberg and Neu (1966), Miller and Kannon (1967) and Zentner, MacGregor and Pogson (1971). Though the bidirectional reflectance of magnesium oxide depends upon the age, purity and preparation technique, the references used for comparision do not give all of these. For this reason and the fact that it is difficult to accurately take data from the curves in the references, very close agreement between the various investigators is not expected.

The magnesium used for this experiment was Sargent and Welch cat. no. SC13283-1. Figure A-1 shows the pertinent quantities of the preparation apparatus. Miller and Kannon held the substrate at -7000 volts with respect to the magnesium ribbon and Brandenberg and Neu held the substrate

10cm from the ribbon. Using the apparatus shown in Figure A-1 approximately 1.5mm of MgO was collected on the substrate. Some data taken with this specimen are presented in Figures A-2, along with data from the literature. Data for unpolarized incident energy were calculated from polarized data using equation A-4. This data demonstrate the general validity of the test system.

The repeatability of the system is demonstrated in two ways. Some data at 0.546 and 0.70 microns were taken twice and data at 0.300 , 0.546 and 1.78 microns were obtained by direct measurements and from calculations based on measurements of data using the polarizer. These data are shown in Figures A-3, A-4 and Tables 3, and 15. Table 3 of Chapter 2 which was taken with the lead sulfide cell and the photomultiplier demonstrates the detectors give essentially the same results. The difference in the specular component is caused by the larger solid angle used for the PbS. This is the only test in which the solid angle was different from that given in Table 3. These data show that the measurements are repeatable within about 1%.

Table A-1 gives the list of errors that will be considered in the uncertainty analysis. As shown under the heading source of error, the errors were either estimated or obtained directly from the manufacturer. The analysis of errors are based on typical data at a source zenith of 60 degrees and

detector zenith of 45 degrees.

An error which is usually considered in this type of investigation but not listed in Table A-1 is that due to stray light. This is omitted because the amplifier rejects any signal which is not at the chopper frequency and because no energy can pass through the chopper except the source. Other possible sources of errors are those due to light which is scattered from the optics and reaches the detector, and light that is reflected from the yoke supports and walls. These errors were determined to be very small by placing a shield in different positions around the detector.

In addition to the systematic errors shown, another systematic error due to the earth magnetic field was discovered early in the investigation. The earth magnetic field deflects the electrons in the photomultiplier in such a manner that a 1% error can occur in the data. The error was removed by magnetically shielding the photomultiplier with a shield recommended by RCA.

In order to make corrections for systematic drift in the signal, data were taken at the beginning and at the end of each run for the independent variables. The difference between the signal is the change in signal during the test. In approximately 61% of the runs the signal drifted down and in 31% of the runs the signal remained constant. In the

remainder of runs the signal increased. The average difference between the signal at the beginning and end of a run was approximately 0.05 volts or 0.5%. Based on a run made with all independent variables constant there was no systematic cycling of the signal. Therefore it appears reasonable to make a linear correction to the data for systematic errors due to signal drift. Then for a signal drift of y' and for a set of data consisting of x points, with n denoting any point the systematic error correction is

$$E_n = D_n y_n / D_1 \qquad \text{(A-1)}$$

where

$$y_n = y''(n-1), \quad n = 2, 3, \text{------}x,$$
$$y'' = y'/(x-1).$$

D_1 is the signal at the beginning of the test and D_n is the signal for any point n. y_n represents the drift from the start of the test until point n. The equation for E_n is based upon the fact that the time it takes to obtain a datum for a given run is approximately the same for all data and the percent change in signal is the same for all data. y_n/D_1 represent the percent change for the n^{th} point during the time it takes to obtain n points.

While taking preliminary data, polarization of the source over the entire spectrum was discovered. The degree

of polarization is shown in Table 27 under the heading source $-D_p/D_s$. The bulk data were taken at 0.300, 0.546 and 1.78 microns without using the polarizers. To determine the effect of source polarization data at a source incident angle of 60 degrees were taken with the polarizers. The reflectance for an unpolarized source is computed as the average of this data according to the equation

$$\rho(\psi,\zeta;\theta,\phi) = \frac{\rho_p(\psi,\zeta;\theta,\phi) + \rho_s(\psi,\zeta;\theta,\phi)}{2} \qquad \text{(A-2)}$$

In terms of measured quantities the unpolarized reflectance is

$$\rho_n(\psi,\zeta;\theta,\phi) = \frac{\frac{D_p(\theta)}{D_p(0°)}\, D_p(0) + \frac{D_s(\theta)}{D_s(0°)}\, D_s(0°) \times P}{D_p(0°) + D_s(0°) \times P} \qquad \text{(A-3)}$$

$$= \frac{\rho_{np}(\theta)D_p(0°) + \rho_{ns}(\theta)D_s(0°) \times P}{D_p(0°) + D_s(0°) \times P} \qquad \text{(A-4)}$$

Where $p \equiv (D_p/D_s)_{source}$

P is used to correct for source polarization. The data in Figures A-3 and A-4 show that source polarization has little effect on the reflectance for the wavelengths in

which the bulk data were taken. For the diffuse data above 0.400 microns a 100% polarized source caused on the average a 5% error in the unpolarized reflectance. Therefore for a 4% polarized source which is about correct for 1.78 microns the error would be about 0.20%. This Figure is 1.2% for diffuse data below 0.35 microns and 3% for the specular data.

The method used to determine the uncertainty is that described by Holman(5). If a dependent variable w is a given function of n independent variables $x_1, x_2, \text{------}, x_n$ then the uncertainty or error in w defined as δw, is given by:

$$\delta w = \left[\left(\frac{\partial w}{\partial x_1}\delta x_1\right)^2 + \left(\frac{\partial w}{\partial x_2}\delta x_2\right)^2 + \text{--------} + \left(\frac{\partial w}{\partial x_n}\delta x_n\right)^2\right]^{\frac{1}{2}} \qquad \text{(A-5)}$$

where

$\delta x_1, \delta x_2, \text{-------} \delta x_n$ = uncertainties in the independent variables. This equation gives a "Root-Mean-Square" or RMS error.

The types of measurements that were made are measurements of reflectance with and without the polarizers and measurements of the source energy with and without the polarizers.

In order to apply equation A-5 to the errors in Table A-1 it is necessary to determine the change in recorder voltage

due to the errors. For wavelengths above 0.40 microns a 90 degree error in polarizer alignment causes a typical change in the signal of 1.0 volts for the diffuse data and 100 volts for the specular data. The term to be used in equation A-5 for the diffuse data due to polarization alignment is

$$\frac{\partial W}{\partial x}\,\delta x = \left(\frac{1}{90}\right) \times 0.8 = 0.0089 \text{ volts} \qquad \text{(A-6)}$$

For wavelengths below .40 microns this term is

$$\frac{\partial W}{\partial x}\,\delta x = \left(\frac{15}{90}\right) \times 0.8 = 0.133 \text{ volts} \qquad \text{(A-7)}$$

For specular data the term to be used for polarization alignment is

$$\frac{\partial W}{\partial x}\,\delta x = \left(\frac{100}{90}\right) \times 0.8 = 1.11 \text{ volts} \qquad \text{(A-8)}$$

which is valid for all wavelengths.

The incident energy location error affects the optical distance between the specimen and the detector. When the detector is at zero zenith this error has a small affect on the signal and when the detector is at 90 degrees there is a direct relationship between error and optical distance. For this analysis the change in voltage due to incident energy location was computed for an angle of 45 degrees where the

$\pm$ 0.3mm error results in a $\pm$ 0.15mm error in detector optical distance from specimen. The relationship between the detector and optical distance is

$$D_1 = D_0 \left(\frac{r_0}{r_1}\right)^2 \tag{A-9}$$

Then for a typical signal at 45 degrees of 6 volts and a detector optical distance of 200mm the error in the output voltage is

$$D_0 - D_1 = 6 - 6(200/200.15)^2 \tag{A-10}$$

$$= 0.009 \text{ volts}$$

For a 1 degree change in yoke (bidirectional device) alignment or angular setting the signal for diffuse data change by 0.1 volts at 45 degrees. The voltage error to be used in equation A-5 is

$$\frac{\partial W}{\partial x} \delta x = \frac{0.1}{10} \times 012 = 0.92 \text{ volts} \tag{A-11}$$

Except at 0.40 microns where the reflectance drops rapidly the data change very slowly with wavelength and is neglected. For the remainder of parameters listed in Table A-1 there is a direct relationship between the errors and the data. Then the RMS of the errors in volts for diffuse data above 0.400 microns is

$$E = \left[(0.03)^2 + (0.009)^2 + (0.02)^2 + (0.02)^2 + (0.02)^2 + \right.$$

$$\left[(0.02)^2 + (0.025)^2 + (0.005)^2 + (0.025)^2 + (0.025)^2\right]^{\frac{1}{2}}$$

$$= 0.115 \text{ volts or } 1.15\% \qquad \text{(A-12)}$$

which is approximately true for polarized and nonpolarized source. For diffuse data below 0.35 microns this value is

$$E = 0.175 \text{ volts or } 1.75\% \qquad \text{(A-13)}$$

For the specular component the change in reflectance with angle is essentially a step change which vary from about 0.04 volts/degree for data at 30 degrees to about 136 volts/degree for data at 75 degrees. Because of this, the detector was adjusted for the maximum signal when measuring the specular component. Then the predominant error depends on the 0.2 degree alignment and source zenith angle errors. As shown Table 28 the error in specular reflectance for a 0.2 degree error in alignment or source zenith varies from 1.4 percent to approximately 15 percent for data above 0.400 microns.

For measurements of the source, Table A-1 is used to compute the uncertainity if errors due to incident energy location, yoke alignment and angle settings on the yoke are omitted. Thus the RMS error is

$$ES = \left[(0.03)^2 + (0.02)^2 + (0.025)^2 + (0.005)^2 + (0.025)\right]^{\frac{1}{2}}$$

$$= 0.051 \text{ volts or } 0.5\% \qquad \text{(A-14)}$$

Several computations are made using the measured data. After

systematic error corrections are made and the was normalized on the measurement at zero zenith a reflectance was computed which is defined by equation 5. Applying equation A-5

$$ER = E/\cos(\theta) \tag{A-15}$$

The polarization is defined as

$$P = (D_p/D_s)_{source} \tag{A-17}$$

Applying equation A-5 to the RMS error

$$EP = \left[\left(\frac{1}{D_s}\,\delta D_p\right)^2 + \left(\frac{D_p}{D_s^2}\,\delta D_s\right)^2\right]^{\frac{1}{2}}_{source} \tag{A-17}$$

Using typical values for D_s and D_p and the value of ES for D_s and D_p the RMS error can be computed

$$EP = \left[\left(\frac{1}{4.8}0.051\right)^2 + \left(\frac{7.9}{4.8^2}0.051\right)^2\right]^{\frac{1}{2}} \tag{A-18}$$

$$= 0.02 \text{ volts}$$

For the data used P = 1.64 which gives a percent error of

$$EP = \frac{0.02}{1.64} \times 100 = 1.34\% \tag{A-19}$$

Some reflectance values were calculated from polarization data by using equation A-4. Applying equation A-5 to get the RMS error

$$ERN = \left\{\left(\frac{D_p(0°) \times \delta\rho_{np}}{D_p(0°) + D_s(0°) \times P}\right)^2 + \left(\frac{D_s(0°) \times P \times \delta\rho_{ns}}{D_p(0°) + D_s(0°) \times P}\right)^2 +\right.$$

$$\left(\frac{\rho_{np} \times D_p(0°) + \rho_{ns} \times D_s(0°) \times P}{(D_p(0°) + D_s(0°) \times P)^2}\right)^2 \times (D_s(0°)\delta P)^2 +$$

$$\left(\frac{\rho_{ns} \times D_s(0°) \times \delta P}{D_p(0°) + D_s(0°) \times P}\right)^2\Bigg\}^{\frac{1}{2}} \qquad \text{(A-20)}$$

ρ_{ns} and ρ_{np} are referenced to 1 volt so E has to be divided by 10 to get $\delta\rho_{ns}$ and $\delta\rho_{np}$. Using typical values for the parameters for wavelengths above 0.400 microns and applying equation A-5 the RMS error can be calculated

$$ERN = \Bigg\{\left(\frac{13 \times 0.0115}{26.84}\right)^2 + \left(\frac{8.44 \times 1.64 \times 0.0115}{26.84}\right)^2 +$$

$$\left(\frac{(0.583 \times 13 + 0.746 \times 8.44 \times 1.64) \times 8.44 \times 0.02}{26.84^2}\right)^2 +$$

$$\left(\frac{0.746 \times 8.44 \times 0.0115}{26.84}\right)^2\Bigg\}^{\frac{1}{2}} \qquad \text{(A-21)}$$

$$= 0.0091 \text{ or } 0.91\%$$

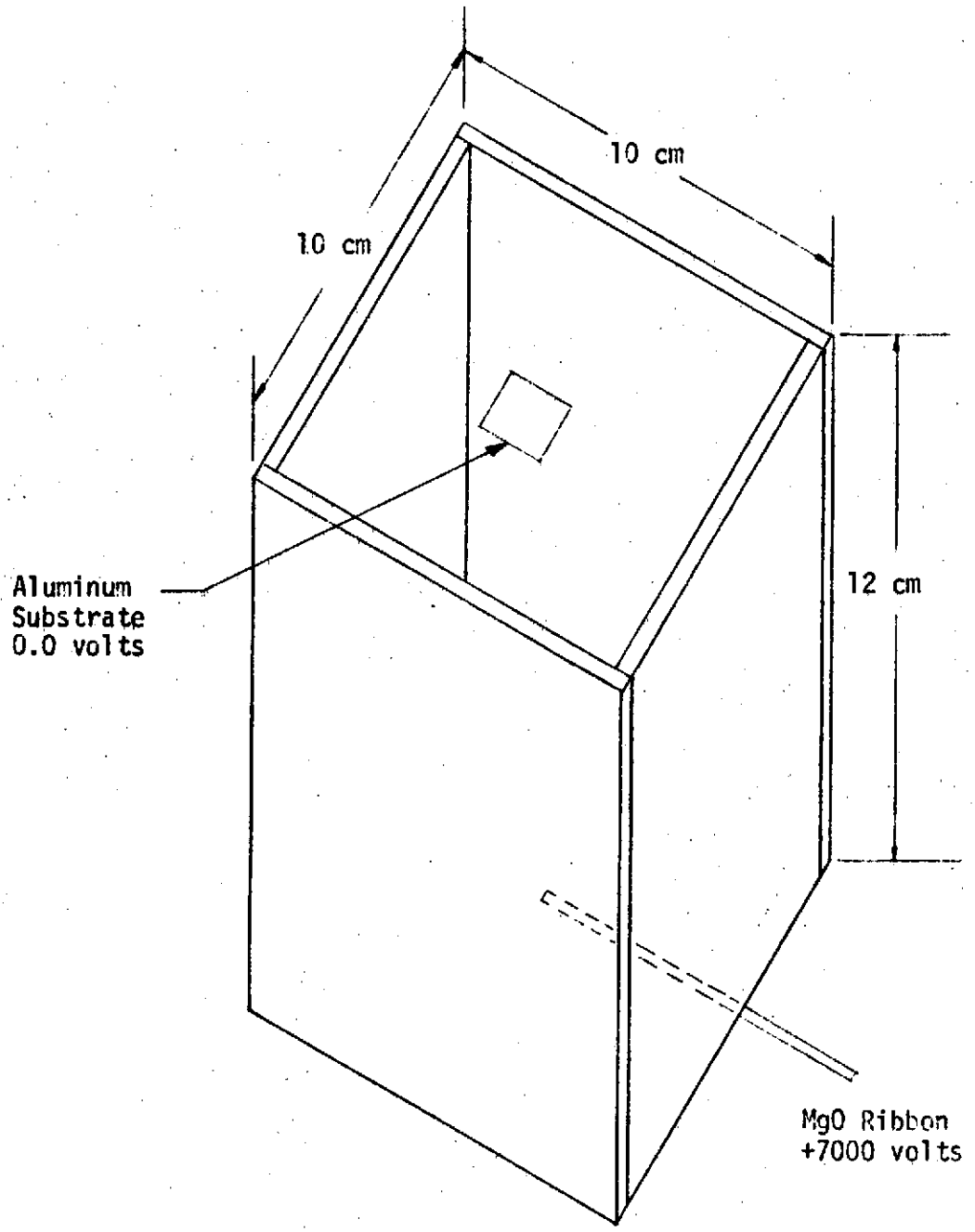

Figure A-1. MgO Preparation Apparatus

TABLE A-1

ERRORS

	Source of Error	Error	Error%
Polarizer Alignment	[1]E	0.8°	[3]0.089%
Nonlinearity of Detectors	[1]M	0.030 volts	0.30%
Incident Energy Location on Specimen @45°	E	0.3mm	0.09%
Yoke Alignment	E	0.20°	0.2%
Angle Settings on Yoke			
a) Detector Zenith	E	0.20°	0.2%
b) Source Zenith	E	0.20°	0.2%
Monochromator Wavelength	E,M	0.001 microns	
Strip Chart Read Out	E	0.02 volts	0.20%
Amplifier Zero Offset	E	0.025 volts	0.25%
Amplifier Nonlinearity	E,M	0.005 volts	0.05%
Instability of Source	E,M	0.025 volts	0.25%
Scattered Light	E	0.025 volts	0.25%
[2]Error due to Source Polarization			
[2]Amplifier Zero Drift	E,M	0.002 volts	0.02%
[2]Drift of PMT or PbS due to Temperature Change			
[2]Change in PMT or PbS Sensitivity due to Bias Volts Change			
[2]Mean Change in Source			
[2]Amplifier Stability			

[1]M-Manufacturer, E-Estimate
[2]Systematic Error
[3]Based on 10 Volts, most Diffuse Data were from 2 to 10 volts.

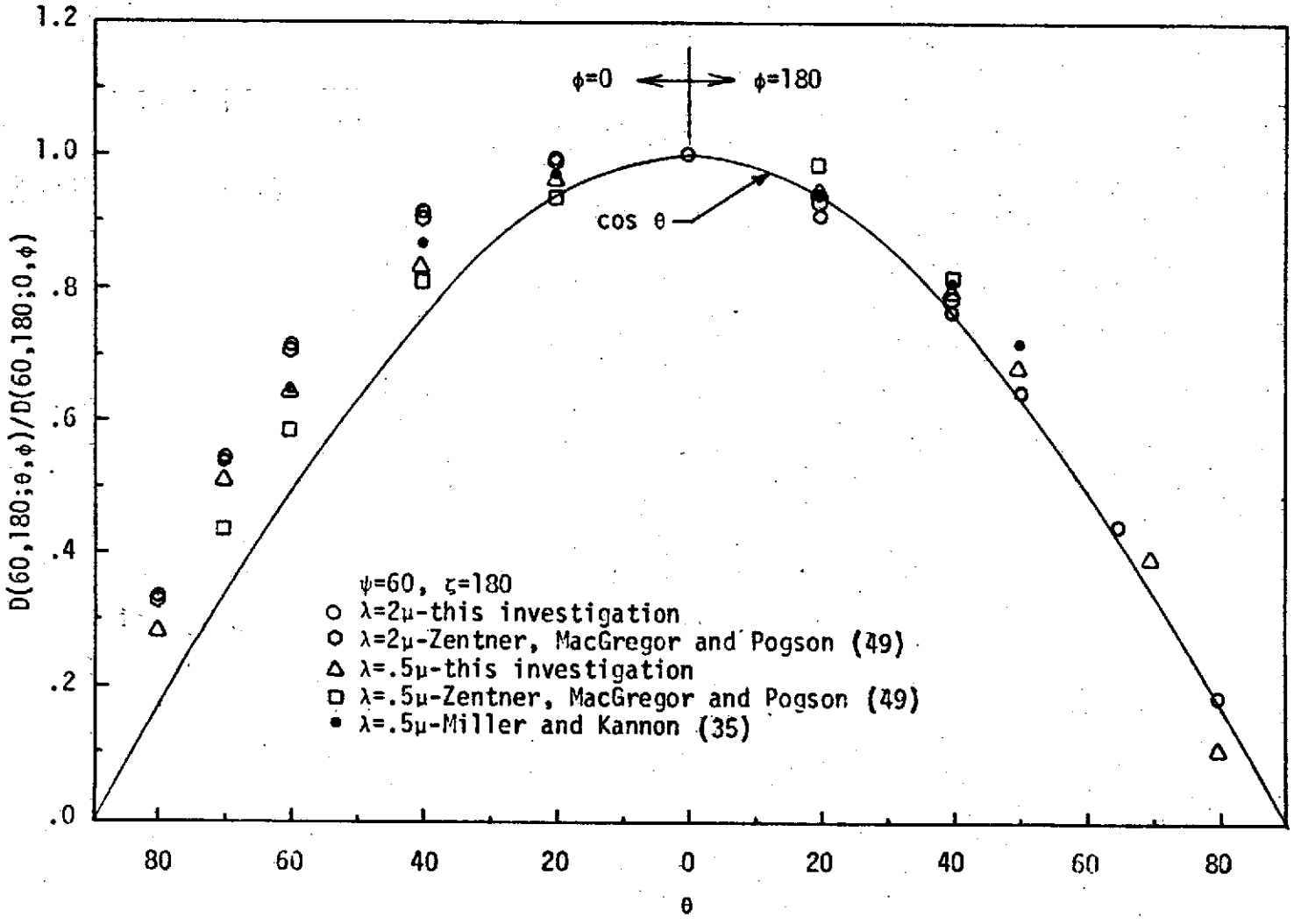

Figure A-2 Reflectance of MgO

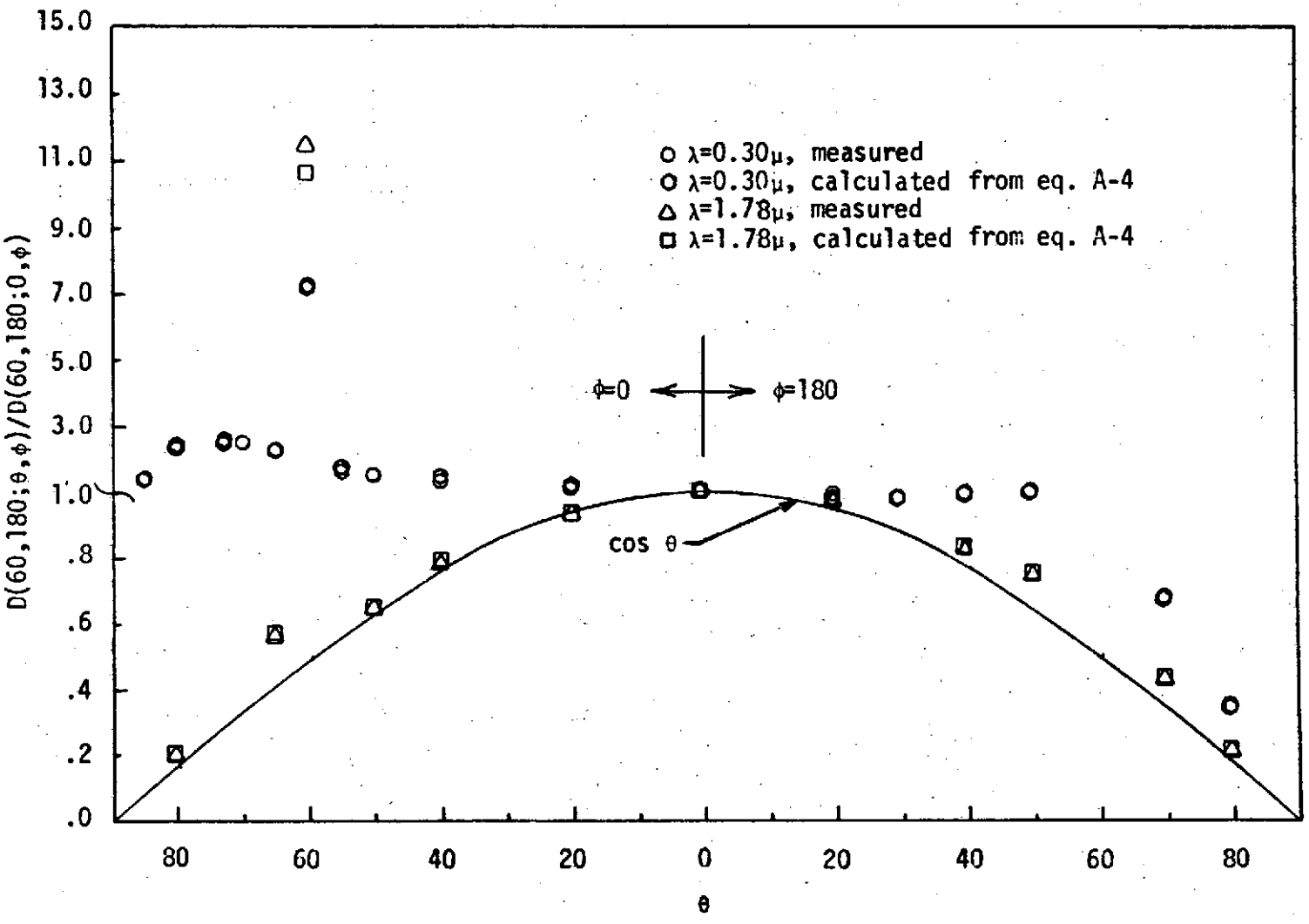

Figure A-3 Reflectance of ZnO

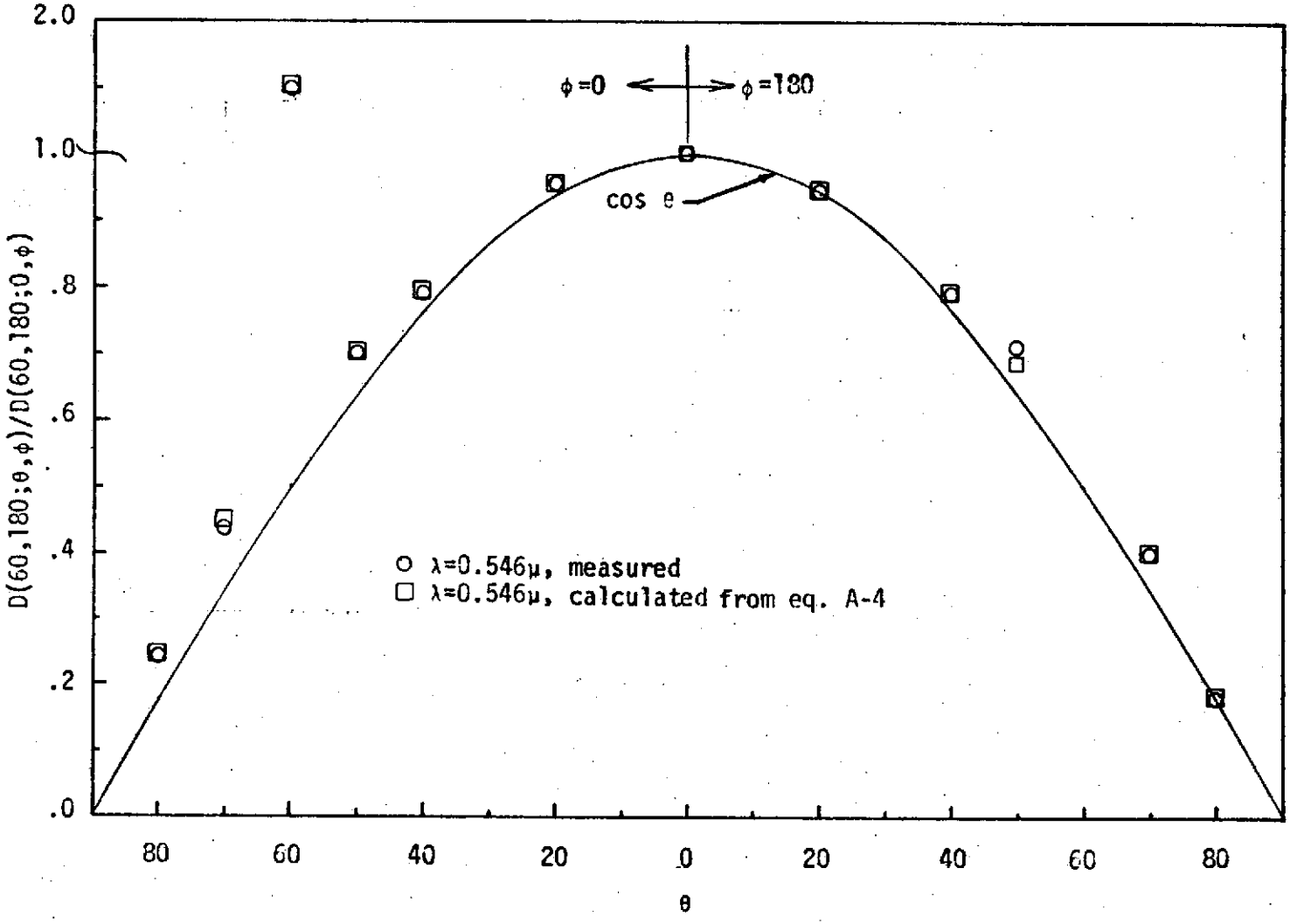

Figure A-4 Reflectance of ZnO

Page intentionally left blank

APPENDIX B

OPTICAL PROPERTIES OF ZnO

The purpose of this appendix is to present some of the optical properties of ZnO used in this investigation. These are the electrical conductivity, index of refraction, transmission, and hemispherical reflection. According to Kroes, et.al. (52) the electrical conductivity of ZnO is 10^{-2} mho cm^{-1} which places ZnO between a conductor (copper, 0.5×10^{10} mho cm^{-1}) and an insulator (glass, 0.5×10^{-7} mho cm^{-1}). This and the data in Table B-1 are used in interpeting the experimental results.

TABLE B-1

PROPERTIES OF ZnO

Wavelength Microns	Index of Refraction Ref. 50 & 54	Transmission* Ref. 55	Hemispherical Reflectance Ref. 56
0.300	-	0.00	7.0
0.370	-	0.00	8.0
0.385	2.44	0.00	-
0.400	2.22	0.00	89.0
0.450	2.11	0.00	93.0
0.500	2.06	2.5	90.0
1.000	1.95	18.0	87.0
1.600	1.93	29.0	90.0
2.000	1.92	30.0	90.0
2.500	1.92	29.0	90.0

*0.76 micron layer formed with a compaction pressure of 11,800 psi.

APPENDIX C

NOMENCLATURE

Arabic Symbols	Quantity	Units
a	Correlation distance of surface height distribution	microns
$\overline{B}$	Magnetic flux density	webers/sq m
C	Capactance	farads
$\overline{D}$	Electric flux density	coulombs/sq m
D	Detector measurement	volts
D_1	Detector signal for r_1	volts
D_o	Detector signal for r_o	volts
$\overline{E}$	Electric field	volts/m
E	Error for diffuse data	volts
E_i	Incident electric field	volts/m
E_n	Systematic error correction	volts
EP	Error in polarization calculation	volts
ERN	Error for diffuse data when calculated from polarization data	volts
E_r	Reflected electric field	volts/m
ES	Error for measurement of source	volts
e_i	Incident energy on specimen	volts
G	Conductance	mhos
$\overline{H}$	Magnetic field	amperes/sq m
I	Current	amperes
$\overline{J}$	Current density	amperes/sq m

NOMENCLATURE (CONTINUED)

Arabic Symbols	Quantity	Units
k	Extinction coefficient	-
L	Inductance	henries
$\bar{T}$	Displacement vector	meters
n	Index of refraction	-
P	Polarization-$(D_p/D_s)_{source}$	-
Q	Charge	coulombs
r_o	Optical distance of detector from specimen	cm
r_1	Optical distance of detector from specimen	cm
S	Closed surface	sq m
t	Time	seconds
V	Electromotive force	volts
w	Any dependant variable	
x	Any independant variable	

Greek Symbols		
ε	Permittivity	farads/m
ς	Source azimuth	degrees
θ	Detector zenith	degrees
θ_r	Reference detector zenith	degrees
λ	Wavelength	microns
μ_1	Permeability	henries
ν	Electromagnetic frequency	Hz

NOMENCLATURE (CONTINUED)

Greek Symbols	Quantity	Units
ρ	$\rho_n/\cos(\theta)$	-
ρ_{ah}	Angular hemispherical reflectance	-
$\rho_{l,d}$	Diffuse bidirectional reflectance	-
ρ_o	Plane reflector reflectance	-
ρ_n, ρ_r	Relative bidirectional reflectance	-
ρ_l	Bidirectional reflectance	-
σ	Peak to valley roughness	microns
σ_o	RMS roughness height	microns
σ_l	Electrical conductivity	coulombs/sq m
ϕ	Detector azimuth	degrees
ϕ_r	Detector reference azimuth	degrees
ψ	Source zenith	degrees
ω_i	Incident solid angle	steradians
ω_r	Reflected solid angle	steradians

Subscripts

p	P-Plane	-
s	S-Plane, Specular component	-

SELECTED BIBLIOGRAPHY

GENERAL

1. Blan, Henry and Fischer, Heinz, Editors. Radiative Transfer From Solid Materials. New York: The Macmillan Co., 1962.

2. Hackforth, H. L. Infrared Radiation. New York: McGraw-Hill Book Company, Inc., 1960.

3. Hadni, A. Essentials of Modern Physics Applies to the Study of the Infrared. New York: Pergamon Press, 1967.

4. Harrison, George R., Lord, Richard and Bourow, John Loop. Practical Spectroscopy. New Jersey: Prentice Hall, Inc. 1948.

5. Holman, J. P. Experimental Methods for Engineers. New York: McGraw-Hill Book Co. 1966.

6. Jenkins and White. Fundamentals of Optics. New York: McGraw-Hill Book Co., Inc., 1957.

7. Koller, L. R. Ultraviolet Radiation. New York: John Wiley and Sons, Inc.

8. Kortum, Gustav. Reflectance Spectroscopy. New York Springer Verlag Inc., 1969.

9. Kruse, P. W., McGlauchin, L. D. and McQuistan, R. B. Infrared Technology. New York: John Wiley and Sons, 1962.

10. Lipson, S. G. and Lipson, H. Optical Physics. Cambridge, Massachusetts: University Press, 1969.

11. Rumshiskii, L. Z. Elements of Probability Theory. New York: Pergamon Press, 1965.

12. Smith, R. A.,Jones, F. E. and Chasmar, R. P. The Detection and Measurement of Infrared Radiation. Oxford: Oxford University Press, 1968.

13. Sparrow, E.M. and Cess, R. D. Radiation Heat Transfer. California: Brooks/Cole Pub. Cp.,1966.

14. Toison, M. La. Infrared and Its Thermal Applications. The Netherlands: N. V. Phillips Cloeilampenfabriek Eindhoven, 1964.

15. Vasko, Antonin, D.Sc. Infrared Radiation. London: Iliffe Book Ltd, 1968.

16. Wendlandt, Wesley Wm. and Hecht, Harry G. Reflectance Spectroscopy. New York: Interscience Pub., 1966.

17. Wiebelt, J. A. Engineering Radiation Heat Transfer. New York: Holt, Rinehart and Winston, 1966.

BIDIRECTIONAL

18. Adorjan, A. S. and Wierum, F. A. "Radiative Properties of Rough Surfaces," Journal of American Institute of Aeronautics and Astronautics, Vol. 9, (November, 1971), pp. 2172-2179.

19. Beckmann, P. and Spizzichino, A. The Scattering of Electromagnetic Waves from Rough Surfaces, New York: Pergamon Press, 1963.

20. Birkebak, R. L. and Eckert, E.R.G. "Effects of Roughness of Metal Surfaces on Angular Distribution of Monochromatic Reflected Radiation." Transactions of the Society of Mechanical Engineers, Series C; Journal of Heat Transfer, Vol. 87, No. 1, (February, 1965), pp. 85-91.

21. Brandenberg, W. M. and Neu, J. T. "Unidirectional Reflectance of Imperfectly Diffuse Surfaces." Journal of Optical Society of America, Vol. 56, No. 1, (January, 1966), pp. 97-103.

22. Chasbane, G., Pieroway, Captain C., and Francis, J. "Reflectance Measurements of Dielectric Coatings on a Conductor Substrate." American Institute of Aeronautics and Astronautics 6th Thermophysics Conference; Tullahoma, Tennessee, April 26-28, 1971, available from Technical Information Service, 750 3rd Avenue, New York, New York A 71-26233.

23. Cox, Roy L., "Radiant Emission from Cavities in Scattering and Absorbing Media," PhD Dissertation, Department of Mechanical Engineering, Southern Methodist University, Dallas, Texas, October, 1968.

24. Davis, H. "The Reflection of Electromagnetic Waves from a Rough Surface." Proceedings of the Institution of Electrical Engineering Part IV, Vol. 101, 1954, pp. 209-214.

25. Eckert, E.R.G. "Messung'der Reflexion Von Warmstrahlen an Technischen Oberflachen." Forschung Auf Dem Gebiete Des Ingenieurwesens. Vol. 7, 1936, p. 265.

26. Hering, R. G. and Smith T. F. "Apparent Radiation Properties of Rough Surface." American Institute of Aeronautics and Astronautics Progress in Astronautics and Aeronautics Thermophysics: Application to Thermal Design of Spacecraft. Vol. 23, edited by J. T. Bevans, New York: Academic Press, 1970, p. 337.

27. Herold, L.M. and Edward, D. K. "Bidirectional Reflectance Characteristics of Rough Sintered Metal and Wire Screen." Journal of American Institute of Aeronautics and Astronautics. Vol. 4, No. 10, October, 1966.

28. Hottel, H. C., Sarofim, A.F., Dozell, W. H., and Vasalos, I.A. "Optical Properties of Coatings Effect of Pigment Concentration." American Institute of Aeronautics and Astronautics 5 th Thermophysics Conference, Los Angeles, California, (June, 1970).

29. Houchens, A. and Hering, R.G. "Bidirectional Reflectance of Rough Metal Surfaces." American Institute of Aeronautics and Astronautics progress in Astronautics and Aeronautics: Thermophysics of Spacecraft and Planetary Bodies (G.B. Heller Ed.) New York: Academic Press, Vol. 20, 1967, pp. 65-69.

30. Leader, J. C. "Bidirectional Scattering of Electromagnetic Waves from Rough Surfaces." Journal of Applied Physics. Vol. 42, No. 12, (November, 1971).

31. Loehnleir, J. E., Winter, E.R.F. and Viskanta, R. "Measurement of Bidirectional Reflectance using a Photographic Technique." American Institute of Aeronautics and Astronautics Paper No. 70-859.

32. Look, Jr., D. C. and Love, T.J. "Investigation of the Effect of Surface Roughness upon Reflectance." American Institute of Aeronautics and Astronautics 5th Thermophysics Conference, Los Angeles, California, June, 1970.

33. Love, T.J. and Francis, R.E. "Experimental Determination of Reflectance Function of Type 302 Stainless Steel." American Institute of Aeronautics and Astronautics progress in Astronautics and Aeronautics: Thermophysics of Spacecraft and Planetary Bodies, (G. B. Heller, Ed.), New York: Academic Press, Vol. 20, 1967, pp. 115-135.

34. Middleton, W.E.K. and Mungail, A.G. "The Luminous Directional Reflectance of Snow." Journal Optical Society of America, Vol. 42, 1952, p. 572.

35. Miller, E. R. and Kannon, R. S. Vun. "Development and Use of a Bidirectional Spectroreflectometer." American Institute of Aeronautics and Astronautics: Thermophysics of Spacecraft and Planetary Bodies (G.B. Heller, Ed.) New York: Academic Press, Vol. 20, 1967, p. 219.

36. Munch, B. "Directional Distribution in the Reflection of Heat Radiation and Its Effects on Heat Transfer." National Aeronautic and Space Administration TTF-497, 1968.

37. Neu, J. T. and Dummer, R. S., "Theoretical and Practical Implications of the Bidirectional Reflectance of Spacecraft Surfaces," National Aeronautic and Space Administration, Contract NAS9-4814, MSFC, Houston, Texas.

38. Nicodermus, F.E. "Directional Reflectance and Emissivity of an Opaque Surface. "Applied Optics, No. 4, 1965, pp. 767-773.

39. Oetking, Philip, "Photometric Studies of Diffusely Reflecting Surfaces with Application to the Brightness of the moon." Journal of Geophysical Research. Vol. 71, No. 10, (May, 1966), pp. 2205-13.

40. Ranau, J. and Collinsor, J.A. "Measurement of Electromagnetic Backscattering from Known Rough Surfaces." Bell System Journal, Vol. 44, 1965, pp. 2203-26.

41. Smith, A. M., Muller, P.R., Tempel Meyer, K. E., and Wood, B.E. "Angular Distribution of Visible and Near IR Radiation Reflected from CO_2 Cryodeposits." Journal of American Institute of Aeronautics and Astronautics, Vol. 7, (December, 1969), pp. 2279-80.

42. Smith, T. F. and Hering, R. E. "Bidirectional Reflectance of a Randomly Rough Surface." AIAA 6th Thermophysics Conference, 1971, Available from Technical Information Service, A71-26246.

43. Spetner, L. M. "Discussion of Davies, H. (1954)." Proceeding of Institute of Electrical Engineers, PT III 102, 148, 1955.

44. Torrance, K.E. and Sparrow, E.M. "Biangular Reflectance of an Electric Nonconductor as A Function of Wavelength and Surface Roughness." Transactions of the American Society of Mechanical Engineers, Series C; Journal of Heat Transfer, Vol. 87, No. 2 (May, 1965), pp. 283-292.

45. Torrance, K. E. and Sparrow, E. M. "Off-Specular Peaks in the Directional Distribution of Reflected Thermal Radiation," Transactions of the American Society of Mechanical Engineers, Series C; Journal of Heat Transfer, Vol, 88, No. 2,(May, 1966), p. 223.

46. Treat, C. H. and Wildin, M. W. "Investigation of a Model for Bidirectional Reflectance of Rough Surfaces," AIAA Progress in Astronautics and Aeronautics: Application to Thermal Design of Spacecraft. Vol. 23, edited by J.T. Bevans, New York: Academic Press, 1970, p. 77.

47. Voshvillo, N. A. "Reflection of Light by a Rough Glass Surface at Large Angles of Incidence of the Illuminating Beam," Optics and Spectroscopy, Vol. XXII, No. 6, (June, 1967), pp. 517-520.

48. Winter, E.R.F., Viskanta, R. and Wen, A. "A Photographic Bidirectional Reflectometer," Warme and Stoffubertagung, Ed. (1968) pp. 95-97.

49. Zentner, R. C., MacGregor, R. K, and Pogson, J. T. "Bidirectional Reflectance Characteristics of Integrating Sphere Coating," AIAA 9th Aerospace Sciences meeting, New york, January 25-27, 1971, Available from Technical Information Services, A71-18534.

ZINC OXIDE PROPERTIES

50. Bond, W. L. "Measurement of the Refractive Indices of Several Crystals," Journal of Applied Physics, Vol. 36, No. 5, (May, 1965), pp. 1674-77.

51. Brown, H. E. Zinc Oxide Rediscovered, New York: The New Jersey Zinc Company, 1957.

52. Gilligan, J. E. "The Optical Properties Inducible in Zinc Oxide", Thermophysic of Spacecraft and Planetary Bodies, Progress in Astronautics and Aeronautics, edited by G. B. Heller, Vol. 20, New York: Academic Press, 1967.

53. Kroes, R. L., Kulshreshtha, A. P., Wegner, V. E., Mookherji, T., and Hayes, J. D. "Effects of Ultra Violet Radiation on Zinc Oxide", Heat Transfer and Spacecraft Thermal Control, Progress in Aeronautics and Astronautics, Vol. 24, The MIT Press, Massachusetts, 1971.

54. Park, Y. S. and Schneider, J. R. "Index of Refraction of ZnO", Journal of Applied Physics, Vol. 39, No. 7, (June, 1968) pp. 3049-52.

55. Schatz, E. A. "Effect of Pressure on Reflectance Measurements", Progress in Astronautics and Aeronautics, edited by G. B. Heller, Academic Press, 1967.

56. Zerlaut, G. A. and Courney, W. J. "Space Simulation Facility for in-situ Reflectance Measurements", Progress in Astronautics and Aeronautics, edited by G. B. Heller, Academic Press, 1967.

APPARATUS SPECIFICATIONS

57. Bausch and Lomb Monochromators-Typical Radiant Flux Output Curves, Bausch and Lomb, New York.

58. Bausch and Lomb/Certified-Precision Diffraction Grating, Bausch and Lomb, New York, 1970.

59. Color Filter Glasses, Corning Glass Works, Corning, New York, 1970.

60. Ealing Science Teaching Catalog, The Ealing Corporation, 1972, p. 163.

61. Grating Monochromators, Bausch and Lomb, New york.

62. Infratron Products Catalog Handbook, Infrared Industries, Inc., Mass.

63. Instruction and Maintenance Manual — Ithaco Model 391A Dynatrac TM Lock-in Amplifier, Ithaca, New York, 1973.

64. Instruction Manual — Mechanical Light Chopper - Model 125, Princeton Applied Research Corporation, New Jersey, 1969.

65. Operating and Service Manual - DC Power Supply, HVB Series, Model 6515A, Serial number prefix 6C, Hewlett Packard, 1967.

66. Polarized Light, Polaroid Corporation, Massachusetts, 1970.

67. RCA Photomultiplier Manual PT-61, Radio Corporation of America, New Jersey.

68. Technical Data for Southern University, P. O. 102633A Spectrum Systems Division, Barnes Engineering Company, Massachusetts, 1973.